Ore Geology Reviews 104 (2019) 227–245

Contents lists available at ScienceDirect

Ore Geology Reviews

journal homepage: www.elsevier.com/locate/oregeorev

Distribution of alteration, mineralization and fluid inclusion features in porphyry – high sulfidation epithermal systems: The Chodarchay example, NW Iran

Narges Yasami, Majid Ghaderi*

Department of Economic Geology, Tarbiat Modares University, Tehran, Iran

ARTICLE INFO

Keywords:
Porphyry–epithermal
Mineralization
Alteration
Fluid inclusions
Chodarchay

ABSTRACT

The Chodarchay Cu-Au deposit in northwestern Iran represents an example of the transition from the deep porphyry mineralization stage overprinted by the shallow high-sulfidation epithermal stage in porphyry – high sulfidation epithermal systems. The mineralization at Chodarchay mostly occurred within the Eocene volcanic and volcaniclastic units; some parts are hosted within an Oligocene quartz monzonite intrusion. The porphyry mineralization is mainly associated with a potassic zone in the deepest part of the stock. The potassic alteration is followed by late alteration types of phyllic, argillic and propylitic. The advanced argillic alteration near the surface postdates other alteration types. Based on the phase contents, six types of fluid inclusions are recognized. At depth, the early generation of halite-bearing inclusions that in some places contain opaque daughter minerals indicates a high-density, high-salinity mineralizing fluid. Usual trails of only vapor-rich inclusions in the shallow parts, suggest intense boiling at (or below) this level. Coexisting vapor-rich and halite-bearing inclusions, as well as vapor-rich and type II fluid inclusion assemblages, indicate fluid immiscibility. The distribution of alteration, mineralization, and fluid inclusion features at Chodarchay provides an example for systematic variations from depth to surface in porphyry–epithermal systems.

1. Introduction

A magmatic-hydrothermal system connecting to arc-type magmatism usually comprises a deep magmatic system related to an intermediate intrusion that develops a higher level to a shallower hydrothermal system (Hedenquist and Lowenstern, 1994). Epithermal mineralization is found in the shallower section, whereas porphyry mineralization develops in deeper, magmatic part of the system (Sillitoe, 2010). Preserved systems that show a transition from shallower epithermal to deeper porphyry mineralization are unusual in the Tarom subzone of western Alborz structural zone of northwestern Iran. The Chodarchay with ore reserve of about 3 million tons and 1.27% Cu grade is the only reported example. Little is known about the porphyry potential of the Tarom. The Chodarchay is unique in the Tarom subzone in its genesis, which is a porphyry – high sulfidation epithermal deposit. Epithermal type mineralization overprints porphyry type mineralization at Chodarchay (Yasami et al., 2017) and provides a window for the exploration potential of porphyry systems in Tarom and western Alborz.

The aim of this investigation is to characterize the distribution of the lithology, alteration, ore mineralization, fluid composition; and probable patterns from depth to the surface, finally compiling all data to develop a schematic model for the Chodarchay deposit as an example of porphyry – high sulfidation systems.

2. Geological setting

The Chodarchay Cu-Au deposit is located approximately 50 km east of the city of Zanjan in the volcano-plutonic Tarom subzone, western Alborz structural zone of NW Iran (Nabavi, 1976) (Fig. 1). The Alborz magmatic belt in northern Iran has an E-W orientation 600 km in length and 100 km wide. The Alborz in the hinterland of the Arabia-Eurasia collision zone occurs in the Alpine–Himalayan belt (Nabatian et al., 2014).

Cenozoic successions of the Alborz are represented mainly by marine and subaerial, porphyritic and non-porphyritic massive lava flows of andesite, basaltic andesite and basalt compositions (Aghazadeh et al., 2010). In the northwestern parts of the Alborz, Cenozoic strata were intruded by Upper Eocene and Oligo-Miocene shoshonitic and high-K calc-alkaline plutons, which are typically related to post-

* Corresponding author.
E-mail address: mghaderi@modares.ac.ir (M. Ghaderi).

https://doi.org/10.1016/j.oregeorev.2018.11.006
Received 12 January 2018; Received in revised form 16 September 2018; Accepted 6 November 2018
Available online 07 November 2018
0169-1368/

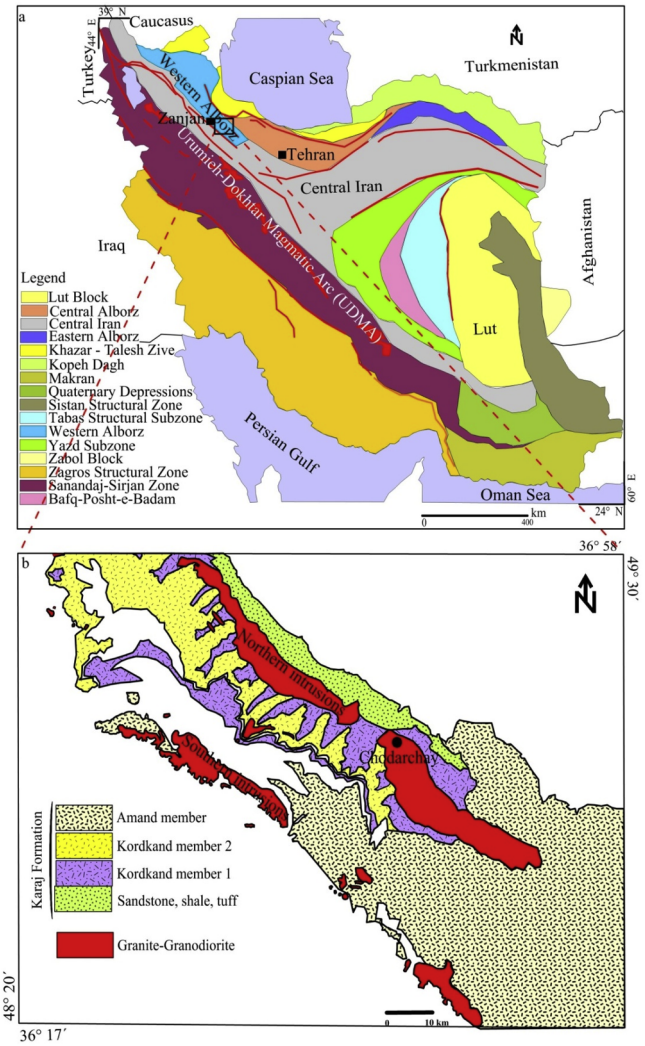

Fig. 1. (a) Simplified structural map of Iran (modified after Sahandi, 2013). Black rectangle represents the location of b. (b) Geological schematic map of the volcano-plutonic Tarom from 1:250,000 geological map of Zanjan (modified after Hirayama et al., 1965, 1966). Tertiary plutonic complex and Karaj Formation are elongated NW–SE. The small black circle shows the location of the Chodarchay area in Fig. 2.

collisional magmatism (Berberian and King, 1981; Aghazadeh et al., 2010; Verdel et al., 2011; Nabatian and Ghaderi, 2013; Nabatian et al., 2014).

Granitoids intruded into the Eocene pyroclastic and lava flows (Karaj Formation) in the Tarom. They form larger plutons in the western and central parts (Castro et al., 2013). The plutonic complex is widespread and forms an elongated NW–SE trending body (Fig. 1). The intrusions show high-K calc-alkaline and shoshonitic affinities and are related to a typical post-collision (Berberian and Berberian, 1981; Nabatian and Ghaderi, 2013).

The study area as part of the Tarom subzone of the western Alborz is mostly composed of lava and pyroclastic rocks (Karaj Formation; Fig. 1) later followed by the intrusion of plutonic rocks. Hirayama et al. (1966) divided Karaj Formation in Tarom into the Kordkand and the Amand members; both composed of volcanic, sedimentary and pyroclastic units. The Amand, which lay upon the Kordkand, is absent in the study area. Four of the Kordkand five units outcrop in the Chodarchay (Fig. 2) and consist mainly of alternating pyroclastic rocks and lava flows. Intermediate to acidic compositions are dominant in the study area.

In the Chodarchay, the plutonism consists of two intrusions; the first one is a broad suite of quartz monzonite to alkali granite, and the second is an alkali granite porphyry stock. The latter is younger because while intruding, it has broken the quartz monzonite margins into pieces.

3. Geology of the Chodarchay

The Chodarchay constitutes the first reported example of the intimate spatial association of high-sulfidation epithermal and porphyry Cu systems in the Tarom (Yasami et al., 2017). The oldest sequence in the area is an Eocene volcanic–pyroclastic complex (Karaj Formation), consisting of rhyolitic crystal and lithic crystal tuff, rhyolite, andesite, and trachyte. Late Eocene–post-Eocene intrusions intruded this sequence as stocks (Fig. 2). The Chodarchay is associated with a shallow quartz monzonite crumbled by younger late alkali granite. Both intrusive bodies are younger than the Karaj Formation units. Hydrothermal alteration types are potassic, phyllic, argillic, propylitic and advanced argillic.

Two types of porphyry and epithermal mineralization have been identified. The latter superposed upon the early one. The ore body is hosted by quartz monzonite and Karaj Formation. The quartz monzonite is the main host to the porphyry mineralization. Mineralization is found mainly as vein-veinlet, disseminated and breccia. Minerals such as enargite, covellite, and bornite which are typical of high-sulfidation mineralization (Einaudi et al., 2003) are less abundant, showing a deeper erosional level.

The major structure is the Chodarchay Fault with an axis oriented at NW 40 (Fig. 2). The ore bodies formed mainly in the direction of the NW fault zone, which most apparently played a consequential role in the lateral migration of the mineralizing fluids.

4. Methods and materials

4.1. Field surveys and subsurface sampling

Field surveys were conducted as part of a study that concentrated on the epithermal and porphyry systems in the area. Samples were collected from the exploration galleries; as well as 1400 m of drill cores from 27 holes. A few suites of fresh and altered samples were collected from the intrusions and surrounding units and mineralized parts in outcrops and drill cores. Core samples from various depths were collected for petrography, mineralography and laboratory analyses. Distribution of lithologic units, alteration types, mineralization zones and fluid inclusions has been examined to define distribution patterns. Based on the above studies, a geological map in the scale of 1:2000 was prepared for the Chodarchay area.

4.2. Analytical methods

Of a few hundred field samples, suitable specimens were chosen. To scrutiny of ore-related metals, samples were collected from drill holes. Ten polished, 70 thin, 50 thin-polished, and 20 double polished sections were prepared from the intrusive, volcanic and volcaniclastic samples from the surface and the bore holes for microscopic studies. A total of 262 drill core samples were analyzed for base metals. Base metal (Cu, Pb, Zn, and Fe) contents were measured using a Varian 220Z atomic absorption spectrometer at the Laboratory of Madankaran Angouran Company in Behabad, Iran.

4.3. Petrography and mineralogy

Prepared thin, thin-polished and polished sections were studied under reflected light microscopy at Tarbiat Modares University, Tehran, Iran. Ore mineralogy, textures, various generations of minerals, paragenesis and petrography, were examined with all the specifics. Also, double-polished thin sections were petrographically examined. Fluid

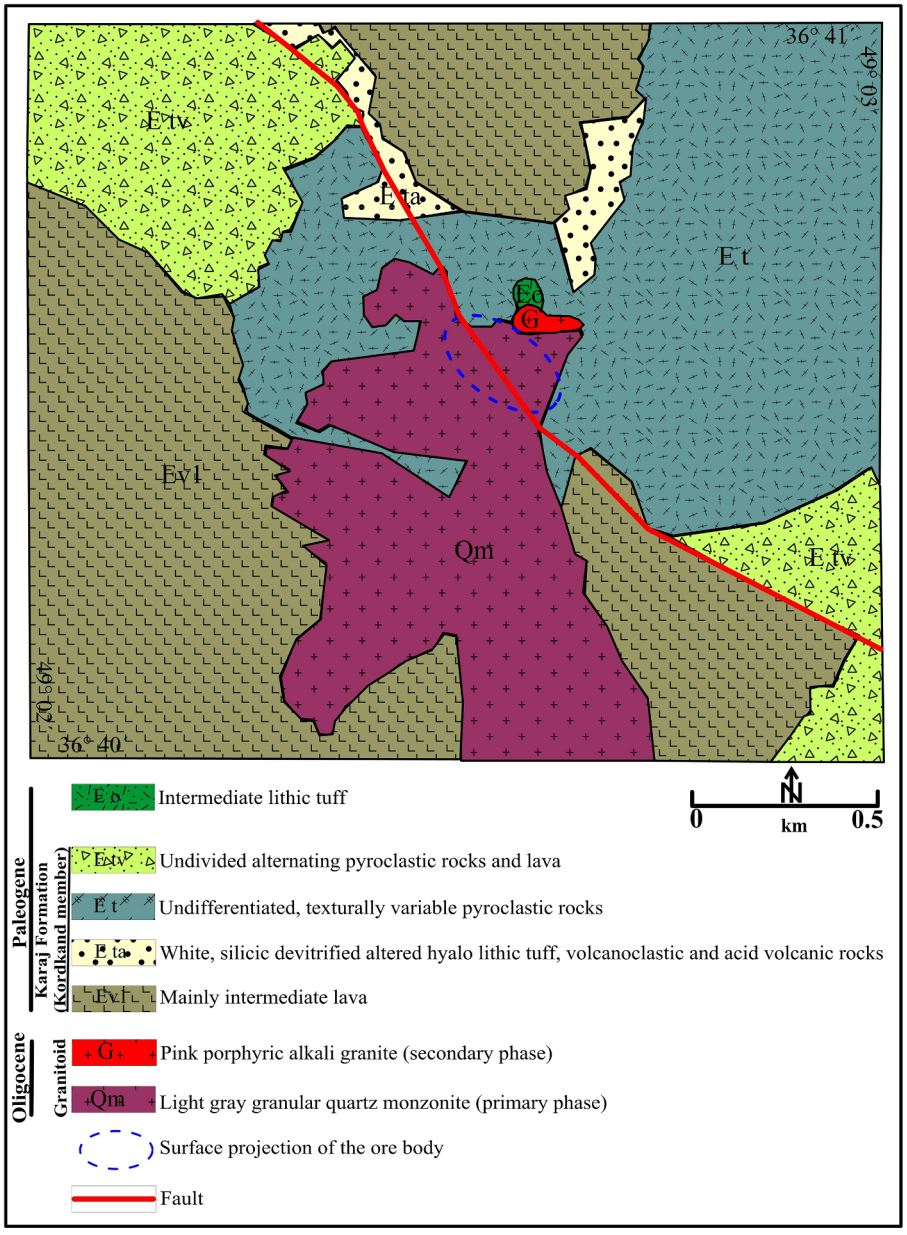

Fig. 2. Geological map of the Chodarchay Cu-Au deposit, Tarom (modified after Yasami et al., 2018).

inclusions in quartz, sphalerite, biotite, and plagioclase were identified, described and classified.

5. Results

5.1. Distribution of rock types

The geology of the area is dominated by volcanic and volcaniclastic sequences. Rhyolite, andesite, trachyte and volcaniclastic units (mainly rhyolitic) (Fig. 3a–d) outcrop in the area. Two types of intrusive stocks are hosted in the Karaj Formation: (1) early quartz monzonite to alkali granite series; and (2) late alkali granite stock (Fig. 3e–h).

Most of the drill cores start with felsic volcanic and volcaniclastic units at the surface and end with quartz monzonite series at depth. The andesite volcanic unit is distal relative to the drilling site, so none of the holes cut it.

Multiple phases of volcanic activity have occurred in the region. Relative dating of the units comes from contact relationships. Magmatic activity is divided into four classes: (1) Eocene lavas and volcaniclastics (Karaj Formation); (2) Late Eocene–post-Eocene quartz monzonite to alkali granite; (3) alkali granite stock that impressed the early intrusion; and (4) late volcaniclastic units that contain lithics from the intrusions.

The small late alkali granite in the northern margin of the quartz monzonite (Fig. 2) with a surface outcrop area of ~0.1 km^2 and its western dike (Fig. 4) crop out just at the surface. The alkali granite is younger enough that has pushed and fractured the quartz monzonite margin and intruded as aplite veinlets into the quartz monzonite (Fig. 5). The quartz monzonite series area is ~0.5 km^2. Since the hydrothermal alteration and mineralization show zoning in the quartz monzonite, it can be suggested that it was effective in alteration and mineralization. Thin section photographs of the two intrusions are presented in Fig. 6.

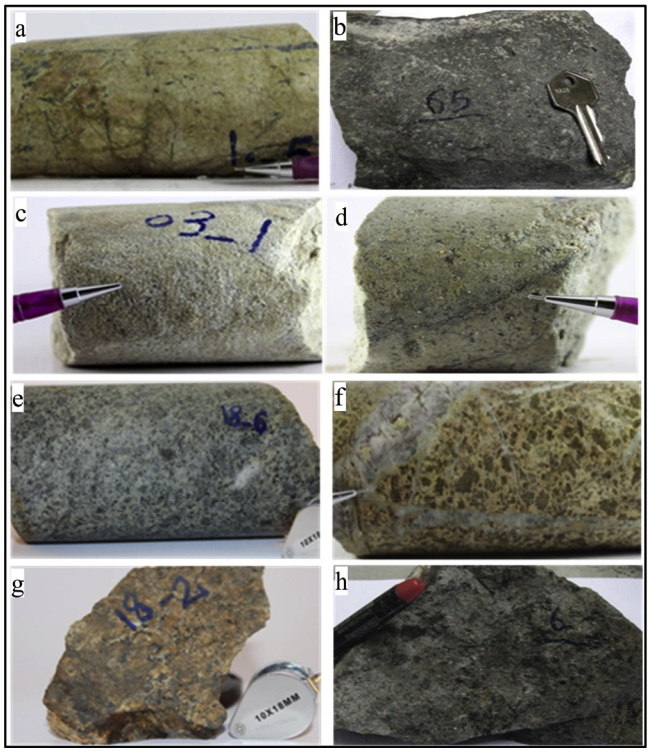

Fig. 3. Macroscopic features of the Chodarchay rock units: (a–d) Lavas and volcaniclastic units: (a) Rhyolite; (b) Andesite; (c) Trachyte; (d) Rhyolitic crystal tuff. (e–h) Intrusive bodies: (e) Quartz monzonite; (f) Early alkali granite; (g) Quartz syenite; (h) Late alkali granite.

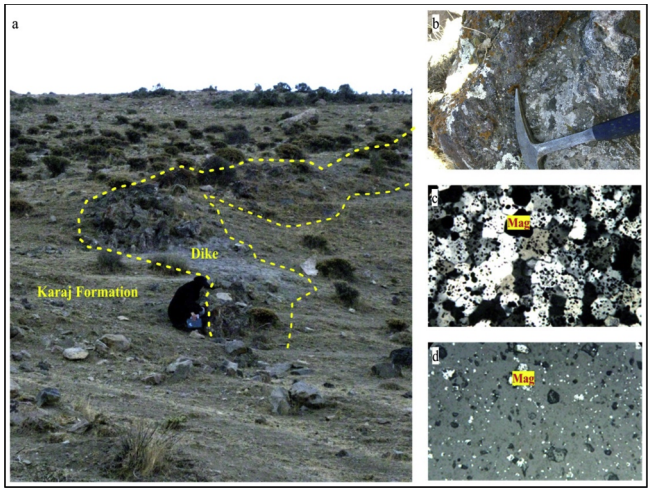

Fig. 4. A dike formed at a later stage as the magma cooled: (a) Outcrop showing the dike intruding into the Karaj Formation; (b) Close-up view of a. (c–d) Microscopic images of the dike from the Chodarchay: (c) In crossed Nicols; (d) In reflected light.

(1) The quartz monzonite as the bottom of the intrusive series displays granular and graphic textures. The major minerals are euhedral to subhedral plagioclase, euhedral to anhedral orthoclase and anhedral quartz. Plagioclase shows polysynthetic twinning (Fig. 6a and b). Euhedral to subhedral hornblende, euhedral clinopyroxene, and subhedral biotite are the minor minerals. Magnetite is the predominant accessory phase. Other accessory minerals include euhedral apatite, euhedral zircon (Fig. 6c), titanite and ilmenite.
(2) The granular quartz syenite part of the series consists of anhedral orthoclase and subhedral quartz as major minerals (Fig. 6d–f).
(3) The early alkali granite as the upper part of the series shows granular and graphic textures. Major minerals consist of subhedral to anhedral orthoclase. Anhedral to subhedral quartz is relatively large. Most of the quartz grains show undulose extinction. The plagioclase is euhedral and shows polysynthetic twinning. The biotite as a minor mineral is subhedral. The hornblende is euhedral to subhedral. Accessory minerals consist of subhedral to euhedral zircon, euhedral titanite, and apatite that occur as inclusions inside the quartz and orthoclase (Fig. 6g–i).
(4) The late alkali granite stock has porphyritic texture and consists of K-feldspar, plagioclase, quartz, biotite, and amphibole. Accessory minerals include magnetite, ilmenite, titanite, apatite, and zircon (Fig. 6j–l).

5.2. Hydrothermal alteration patterns

Hydrothermal alteration in porphyry deposits is usually widespread and has zoning in deposit scale and near the veinlets and fractures (Titley, 1982; Sillitoe, 2000, 2010; Seedorff et al., 2005, 2008; Tosdal et al., 2009). Ideal porphyry deposits are typically described by hydrothermal alteration zonation (Lowell and Guilbert, 1970). Usual alteration zones in porphyry deposits include an inner potassic zone and an outer propylitic zone. Phyllic and argillic zones may have occurred between the potassic and propylitic zones or as younger irregular or tabular zones overprinting the former sulfide and alteration assemblages (Meyer and Hemley, 1967; Sillitoe, 2010).

Hydrothermal alteration has affected volcanic and intrusive rocks at the Chodarchay. Distribution of alteration types in the deposit scale has been studied by petrography of the outcrop and core samples. Spatial progression of alteration types was examined by cross-cutting relationships in hand specimens and their thin sections.

The potassic as the oldest alteration event is developed in the innermost part of the intrusion. The secondary K-feldspar replacing plagioclase and the smaller secondary biotite and magnetite replacing hornblende within the quartz monzonite, indicate to potassic alteration (Fig. 7a). At the Chodarchay, mineralization in this zone can be important as an exploration guide for other possible similar deposits due to the deposit being the first reported porphyry mineralization in the Tarom. The potassic alteration grades to a higher level either to phyllic and then to argillic or directly to the argillic alteration.

Phyllic zone normally overprints potassic and chlorite–sericite alteration assemblages (Dilles and Einaudi, 1992; Sillitoe, 2010). The phyllic assemblage consists of sericite, quartz, and pyrite at the Chodarchay (Fig. 7b). This alteration changes to potassic and chlorite–sericite alteration (Fig. 7c) with an increase in depth.

The phyllic alteration changes upwards to argillic alteration in some cores. In the upper parts of the system, host rocks are thoroughly altered to propylitic or argillic alteration (Fig. 7d). The argillic alteration that is characterized by sericite, clay mineral, and quartz, has affected the intrusion as well as the surrounding rocks.

The propylitic alteration surrounds the other alteration types. The propylitic alteration zone typically consists of chlorite and calcite or epidote (Fig. 7e). The presence of sericite and chlorite in the absence of epidote (Fig. 7c) may equate to the intermediate argillic zone (e.g., Ohio Creek; Brathwaite et al., 2001).

The advanced argillic alteration overprinted on an early-formed alteration halo. In the high-sulfidation environment, ore deposition is thought to be a separate event from early advanced argillic alteration which produces the residual vuggy quartz (Fig. 7f) typical of high-sulfidation epithermal deposits (Arribas, 1995).

The alteration and mineralization at the Chodarchay is the result of hydrothermal activity from the interplay of magmatic fluids from the high-level intrusion and neighboring country rocks. Hydrothermal alteration assemblages at the Chodarchay are described in Table 1.

Leached cap, oxide/sulfide mixture zone and hypogene mineralization zones are regularly distributed at the Chodarchay (Fig. 8). The

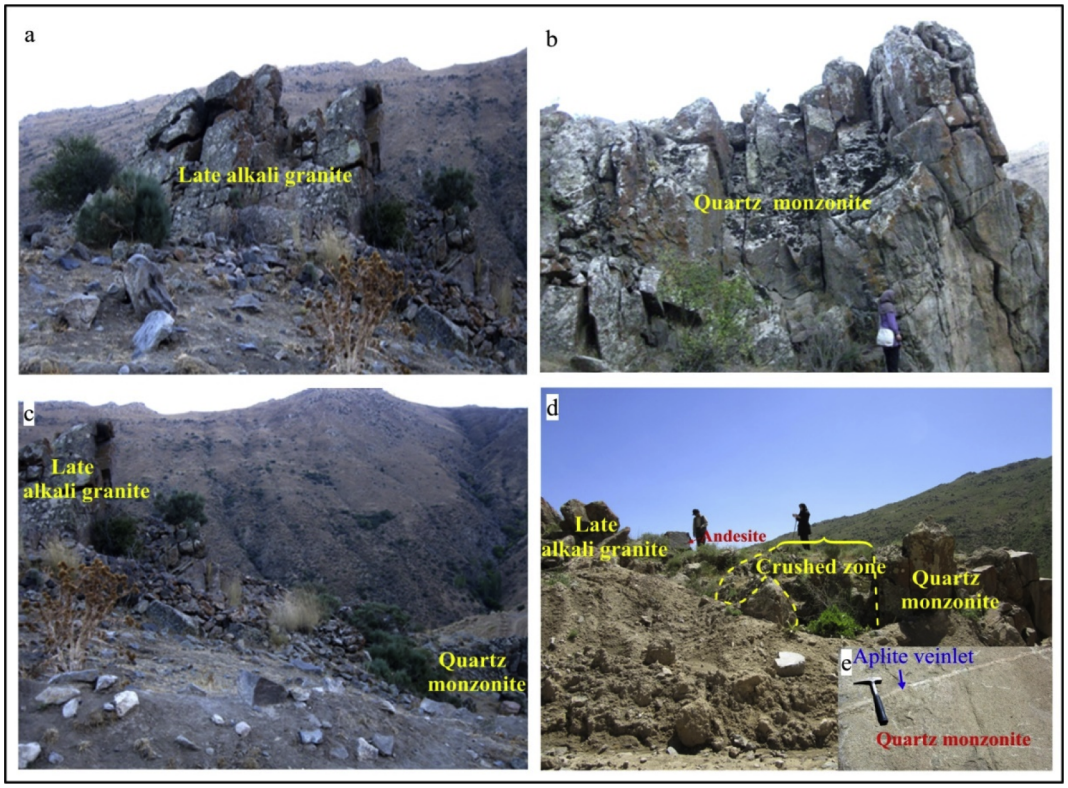

Fig. 5. (a) Late alkali-granite outcropped in the north of the quartz monzonite; (b) Outcrop of quartz monzonite at the Chodarchay; (c) Alkali granite next to the quartz monzonite. left: outcrop image of alkali granite; right: outcrop image of quartz monzonite; (d) Close-up view of c; crushed zone developed along the contact of the two intrusive units; (e) Younger aplitic vein cross-cutting the early quartz monzonite.

leached cap contains abundant oxides and is characterized by high porosity. Coexistence of limonite and sulfides denote oxide/sulfide mixture zone. The hypogene as the deepest zone is without limonite, and other ferro oxy-hydroxy minerals, while sulfides are the dominant ore minerals.

5.3. Mineralization and paragenesis

The mineralization at Chodarchay is characterized by two distinct successive events of ore formation. Late stage high-sulfidation epithermal postdates the previous porphyry mineralization. The mineralization was emplaced within a fault system. Observations reveal an important primary structural control on the mineralization at the Chodarchay (Yasami et al., 2017), associated with little lithological control.

The porphyry mineralization developed within and around the quartz monzonite series. High-sulfidation epithermal is linked with porphyry Cu mineralization (Yasami et al., 2017). This model is based on concepts for epithermal deposits (Hedenquist and Lowenstern, 1994; Hedenquist et al., 2000). The potassic alteration is the pre-epithermal ore hydrothermal activity in the intrusion. Epithermal mineralization postdates the intrusion of a quartz monzonite and is defined as the period of hydrothermal activity that occurred after cessation of the intrusive activity at present levels of exposure and reactivity of the Chodarchay Fault (Yasami et al., 2017).

5.4. Mineralization zoning

The mineralized area is divided into three zones: (1) deeper hypogene sulfides; (2) near-surface enriched supergene sulfides; (3) surface oxidized and leached zone. The most abundant hypogene sulfides are chalcopyrite, pyrite, sphalerite, and galena. The supergene sulfide zone is characterized by chalcocite, digenite, and covellite replacing chalcopyrite, with chalcopyrite relicts observed in many samples. Chalcopyrite is completely or partially replaced by chalcocite, digenite, and covellite. The exposed hypogene sulfides near the surface have been largely oxidized by supergene processes and replaced by Fe-hydroxides, Cu-oxides, Cu-carbonates, and Cu-silicates such as malachite, azurite, hematite, goethite, and limonite to form a leached cap and the oxide zone.

The geometries of mineralization consist of vein-veinlets, mineralized breccias, open space filling, massive sulfides, and dissemination. The vein-veinlet is volumetrically the most important mineralization type. The thickness of veinlets varies from a few cm to several dm. The mineralized breccias are present in all the cores and outcrops. Dissemination is mainly widespread in the phyllic zone; generally, the disseminated mineral is pyrite. In higher levels, magnetite is associated with pyrite. Gold, chalcopyrite, pyrite, sphalerite, galena, bornite, chalcocite, covellite, digenite, copper and iron oxides, malachite, azurite and sulfosalts are the main minerals (Figs. 9 and 10).

5.4.1. Hypogene sulfides

Chalcopyrite is the most abundant ore mineral during the hypogene stage. Three generations of chalcopyrite are present. The first generation occurs as fine-grained and disseminated crystals and veinlet in the porphyry stage (Fig. 9a). The veinlet and open space filling chalcopyrite in the mineralized breccias characterize the second generation (Fig. 9b). Equilibrium boundaries of chalcopyrite, sphalerite, and galena show that they are contemporaneous (Fig. 9c). Epithermal stage chalcopyrite has been replaced in margins and fractures by bornite, chalcocite, covellite, digenite, copper and iron oxides. Malachite and azurite are the other minerals replacing the chalcopyrite. In some microscopic sections, chalcopyrite surrounded automorph pyrite, thus this generation of pyrite formed before the chalcopyrite (Fig. 9d). The latest generation formed by chalcopyrite emulsions inside the sphalerite (chalcopyrite disease) (Fig. 9c).

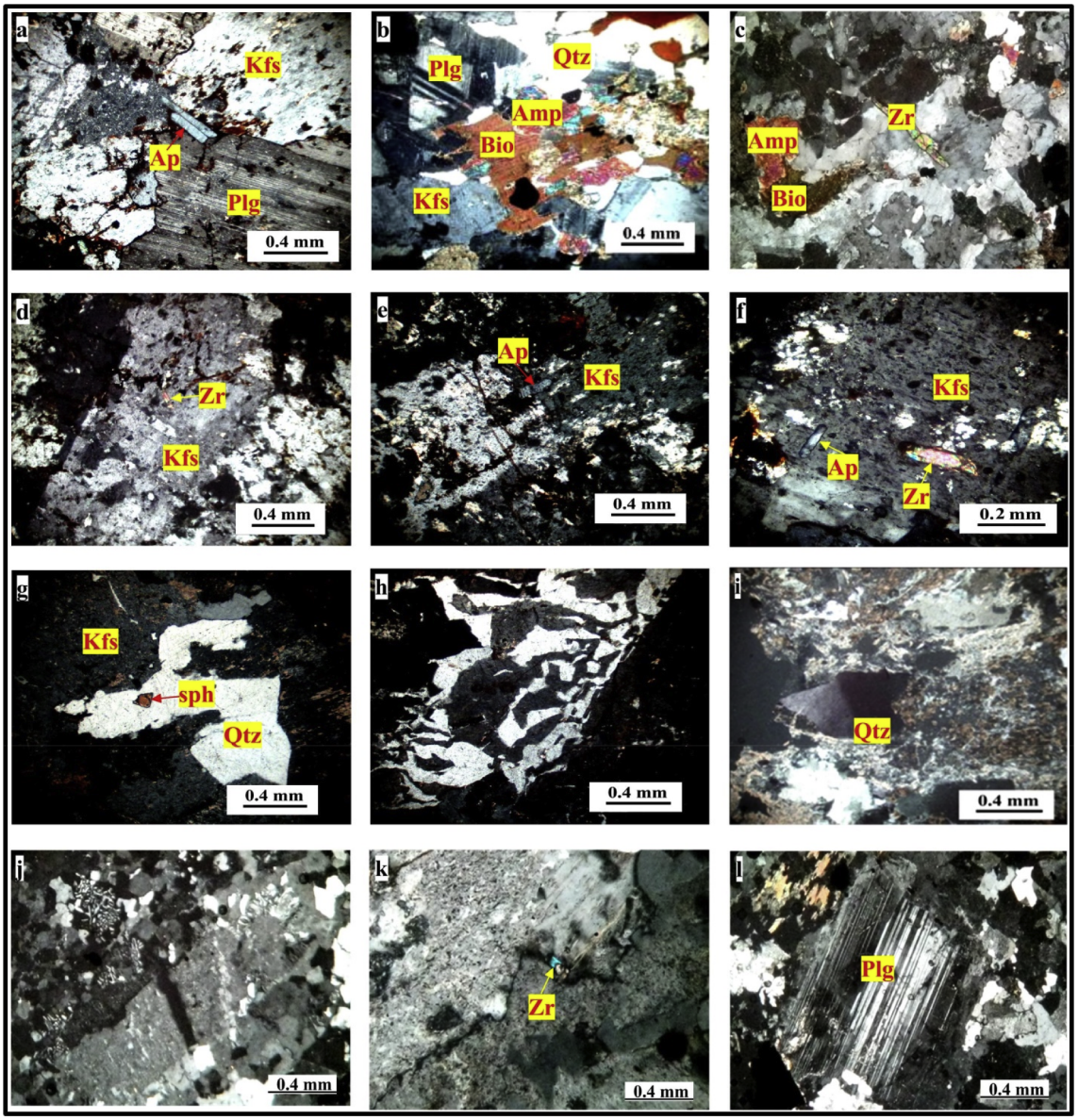

Fig. 6. Thin section photomicrographs showing mineral assemblages and textures in the intermediate-felsic intrusions from the Chodarchay area: (a–c) Representing samples of the quartz monzonite: (a) Apatite needles are found at alkali-feldspar and plagioclase contact margin; (b) Plagioclase, alkali-feldspar, quartz, amphibole, and biotite in quartz monzonite; (c) Euhedral zircon grain within a quartz monzonite. (d–f) Minerals of the quartz syenite unit: (d) Zircon fully enclosed within orthoclase; (e) Elongated apatite within orthoclase; (f) Zircon and apatite inclusions within orthoclase. (g–i) Early alkali granite: (g) Rhombohedral titanite as accessory mineral within quartz in early alkali granite; (h) Black and white graphic texture with intergrowths of quartz and alkali-feldspar; (i) Undulose extinction of quartz in early alkali granite. (j–l) Represent late alkali granite: (j) An intergrowth of quartz and alkali-feldspar (granophyric texture); (k) Zircon inclusion within late alkali granite; (l) The porphyritic texture in late alkali granite. Plagioclase twinning is easily seen using a polarizing microscope.

Pyrite is common in most hydrothermally altered and mineralized rocks and occurs in four generations. Porphyry mineralization related disseminated pyrite shows the first and the oldest generation (I). The second is alteration related very fine to large disseminated crystals of euhedral to subhedral pyrite (II) (Fig. 9e). Mineralization stage euhedral to subhedral pyrites (III) associated with other ore minerals such as chalcopyrite, sphalerite, and galena occur in quartz veinlets and breccia clasts and matrix (Fig. 9d and f). The colloform pyrite is the last generation (IV), some rounded pyrites formed in late stages of the hydrothermal system associated with magnetite show that the hydrothermal fluid was oxidized (Fig. 9g).

Sphalerite and galena occur as veinlets and in quartz veinlets and mineralized breccias isolated or associated with other ore minerals. Galena surrounds sphalerite indicating that galena formation continued after sphalerite (Fig. 9h). Enargite points to the high-sulfidation epithermal mineralization. This mineral is associated with sulfide minerals such as galena and pyrite (Fig. 9i). Tetrahedrite and tennantite occur as amorphous sulfosalt inclusions inside the chalcopyrite and sphalerite (Fig. 9j, k). There is no association between the gold and other ore minerals, and it occurs just inside the quartz (Fig. 9l).

5.4.2. Enriched supergene sulfides

Near the surface, supergene bornite and chalcocite partially replace hypogene sulfide minerals, typically as thin rims near fracturing and outskirt of the sulfides. Supergene chalcocite and bornite have replaced chalcopyrite (Fig. 10a). Covellite associated with digenite replaced chalcopyrite as thin rims (Fig. 10b).

5.4.3. Oxidized and leached zone

The Chodarchay mineralization system has been oxidized and

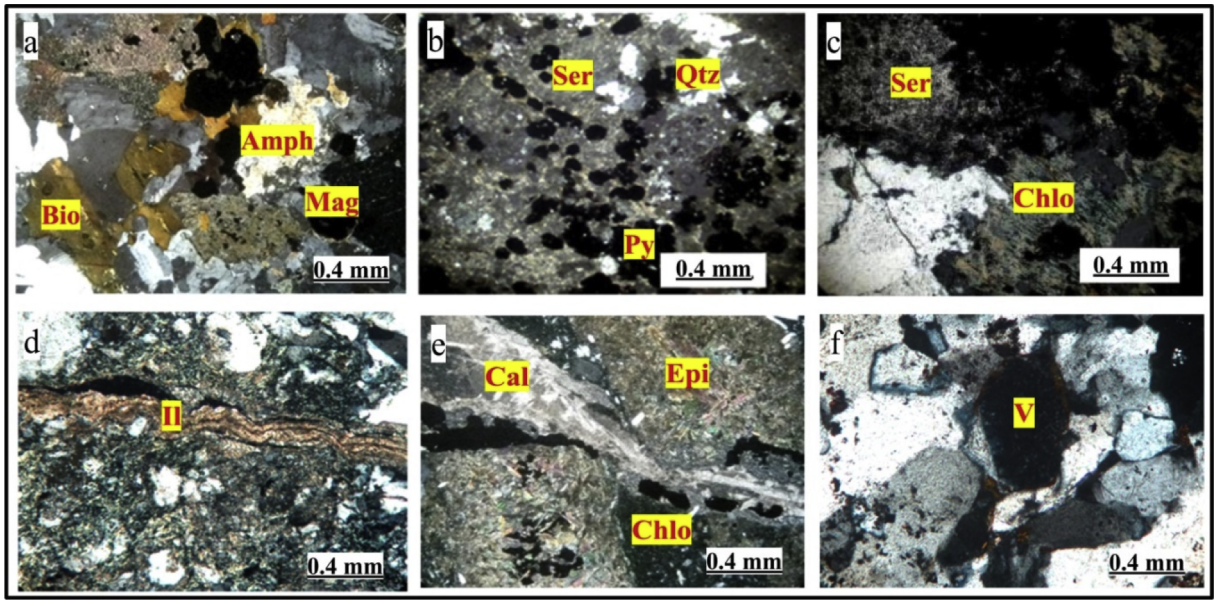

Fig. 7. Hydrothermal alteration associated with the Chodarchay porphyry-epithermal deposit: (a) Brown biotite replaces amphibole (hornblende) in the potassic alteration; (b) Quartz + sericite + pyrite assemblage in phyllic alteration; (c) Chlorite–sericite (intermediate argillic) alteration assemblage; (d) Fine-grained illite (birefringent mineral) in argillic alteration; (e) Epidote + calcite + chlorite assemblage shows propylitic alteration; (f) Vuggy quartz is clearly visible in advanced argillic alteration. Abbreviations: Amph: Amphibole, Bio: Biotite, Mag: Magnetite, Qtz: Quartz, Py: Pyrite, Ser: Sericite, Chlo: Chlorite, Il: Illite, Cal: Calcite, Epi: Epidote, V: Vuggy.

Table 1
Hydrothermal alteration assemblages, alteration types and altered rock units at the Chodarchay deposit.

Alteration minerals	Alteration types	Rock units
Secondary alkali-feldspar, secondary biotite, magnetite	Potassic	Quartz monzonite
Sericite, chlorite	Intermediate argillic	Alkali granite - rhyolite
Sericite, quartz, pyrite	Phyllic	Alkali granite - quartz monzonite – rhyolite - rhyolitic crystal tuff - breccia
Sericite, tourmaline	Sericite-Tourmaline	Alkali granite - rhyolite - breccia
Tourmaline	Tourmaline	Alkali granite - trachyte tuff - rhyolitic crystal tuff - breccia
Sericite-clay associated with disseminated pyrite	Argillic	Alkali granite - breccia
Actinolite, epidote, chlorite, carbonate, pyrite	Propylitic	Alkali granite - quartz monzonite - rhyolite
Kaolin, quartz, alunite	Advanced Argillic	Alkali granite
Quartz	Vuggy quartz	Unknown
Quartz	Siliceous	Alkali granite - quartz monzonite - quartz syenite - rhyolitic crystal tuff - breccia
Carbonate	Carbonated	Alkali granite - trachyte tuff - rhyolite - rhyolitic crystal tuff - breccia

partially leached at the surface (Fig. 8a). Oxide copper minerals (such as malachite and azurite) appear in surface exposures (Fig. 10b and c). Oxidation of hypogene sulfides such as pyrite and oxide minerals such as magnetite produces goethite and hematite (Fig. 10d–f). Bernalite which is a very rare ferric iron hydroxide with a structure related to that of perovskite exists at the Chodarchay. Chemical analyses of this unusual mineral reveal presence of very small amounts of Si, Pb, Zn, H_2O and CO_2 (Birch et al., 1992, 1993; McCammon et al., 1995).

The relative timing of successive events is described by paragenesis. The paragenesis comprises two principal stages clarifying how the porphyry system evolved through high-sulfidation to supergene processes (Fig. 11).

The Chodarchay mineralization system is structurally and morphologically related to the ore-controlling fault with NW-SE trend. There are some lines of evidence for the post-mineral faulting. Pyrite III in some places shows breccias and cataclastic textures that emphasize on post-mineralization structural activity (Fig. 12a). Chalcopyrite has been tectonically brecciated (Fig. 12b). Tectonics affected the galena too, and lead to triangle cleavages elongated (Fig. 12c and d).

5.5. Vein-veinlet classification

Various types of hydrothermal mineralized veinlets were categorized at Chodarchay based on their mineralogy. The main types include: (1) Quartz-sulfide veinlets (e.g., quartz-chalcopyrite veinlets and quartz-chalcopyrite-pyrite veinlets) (Fig. 13a and b); (2) Calcite-sulfide veinlets (e.g., calcite-sphalerite-galena-pyrite-chalcopyrite veinlets) (Fig. 13c); (3) Epidote-sulfide veinlets (e.g., epidote-sphalerite veinlets) (Fig. 13d); (4) Chlorite-sulfide veinlets (e.g., chlorite-sphalerite-galena veinlets; chlorite-chalcopyrite-sphalerite veinlets) (Fig. 13e–g); (5) Sulfide veinlets (e.g., galena-sphalerite-chalcopyrite veinlets, chalcopyrite-pyrite veinlets, chalcopyrite veinlets, pyrite veinlets and galena veinlets) (Fig. 13h–l). The main types are the quartz-sulfide veinlets. Veinlet types associated with their host rocks and related hydrothermal alteration types are presented in Table 2.

5.6. Metal dispersion

Distribution of deposit-scale ore-related metals is shown in Fig. 14.

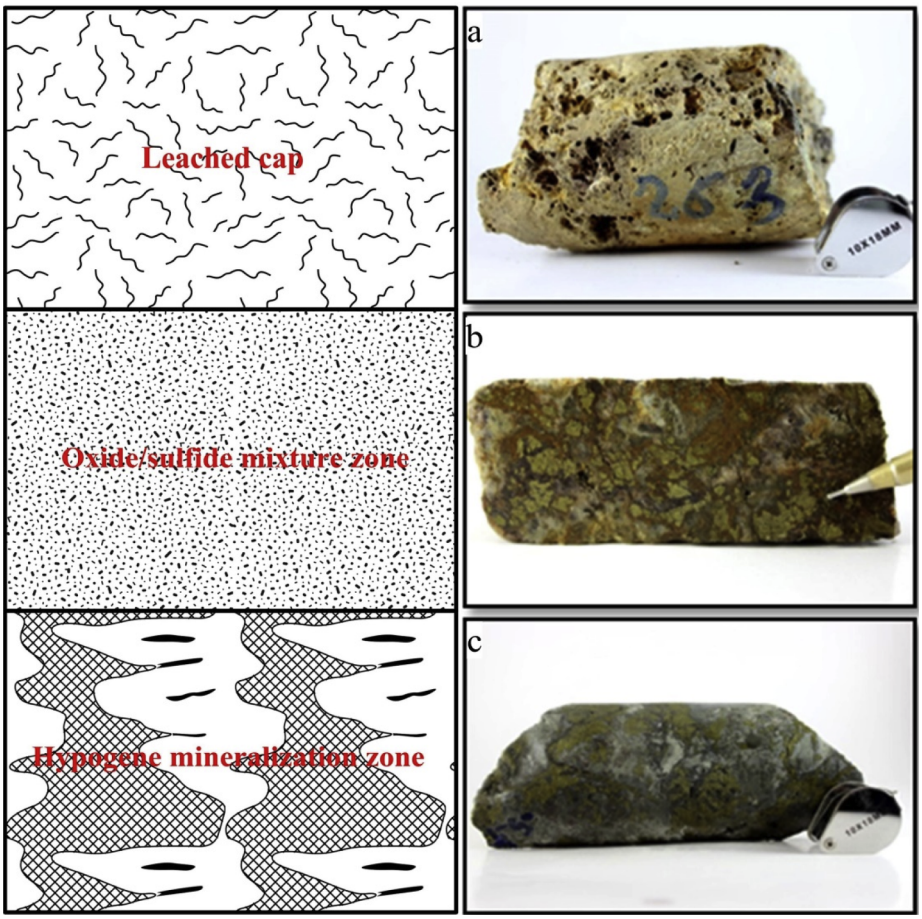

Fig. 8. Distribution of the three zones at the Chodarchay deposit: (a) Leached cap; (b) Oxide/sulfide mixture zone; (c) Hypogene mineralization zone.

Copper grades in the shallow parts are below 0.5%. Zinc grades are mostly below 4.5%, although locally they reach concentrations up to 21%. Lead grades are all below 4.5%. The highest iron grades (between 10 and 22%) are associated with the highest Cu grades in the system. Elevated Cu and Fe grades occur at the shallow parts.

5.7. Fluid inclusions

Numerous studies have been carried out on fluid inclusions in active geothermal systems, their fossil equivalents, and the epithermal precious metal deposits (Kamilli and Ohmoto, 1977; Roedder, 1984; Bodnar et al., 1985; Vikre, 1985; Hedenquist et al., 2000; Albinson et al., 2001; Simmons et al., 2005; Camprubí and Albinson, 2007). The close association between boiling and mineral deposition in the epithermal environment is documented by a large database of fluid attributes (c.f., Brown, 1986).

Petrographic examination of fluid inclusions including identification of daughter minerals and gases, paragenesis of fluid inclusion populations, and recognition of constant or variable phase ratios within populations in hydrothermal and igneous minerals can determine qualitatively the major components, relative ages, and evolution of fluids that formed porphyry deposits (John, 2010).

Fluid inclusions provide the means for investigating the nature and composition of the involved fluids in ore-making processes. Fluid inclusion assemblage (FIA) is a group of fluid inclusions that all form at the same time (Goldstein and Reynolds, 1994). The secondary FIAs at the Chodarchay quartz trapped in repaired fractures. This generation of fluid inclusions is typical in porphyry deposits (Lecumberri-Sanchez et al., 2013).

5.7.1. Distribution of fluid inclusion types

The fluid inclusions are hosted by quartz, biotite, plagioclase, and sphalerite. Six types of fluid inclusions were identified in the host minerals (Fig. 15; Table 3).

5.7.1.1. Fluid inclusion types in the quartz. Veinlet quartz includes small liquid- and vapor-rich two-phase inclusions. Filling quartz includes liquid-rich two-phase, vapor monophase and solid-bearing multiphase inclusions. There are liquid-rich two-phase, vapor-rich two-phase, and halite-bearing multiphase inclusions in the magmatic quartz grains. Six types of fluid inclusions were recognized in the quartz (Fig. 16).

Type I occurs as oval and elongated liquid monophase (up to 20 μm in their maximum dimension) in one sample from about 14 m depth (Fig. 16a).

Type II as oval, square, sphere, elongated and irregular shapes, exists in all depths and is the most abundant type. 20–40% of the volume is occupied by the vapor. These are between 2 and 70 μm in their maximum dimension (Fig. 16b).

Type III is in oval, rhombic, irregular and negative crystal shapes and between 3 and 60 μm. The vapor occupies 60–90% of the volume and in some cases more than 90% (Fig. 16c).

Type IV as oval, rhombic and negative crystal shapes and are vapor-rich (Fig. 16d).

Type V as oval, square, rectangular and irregular forms are

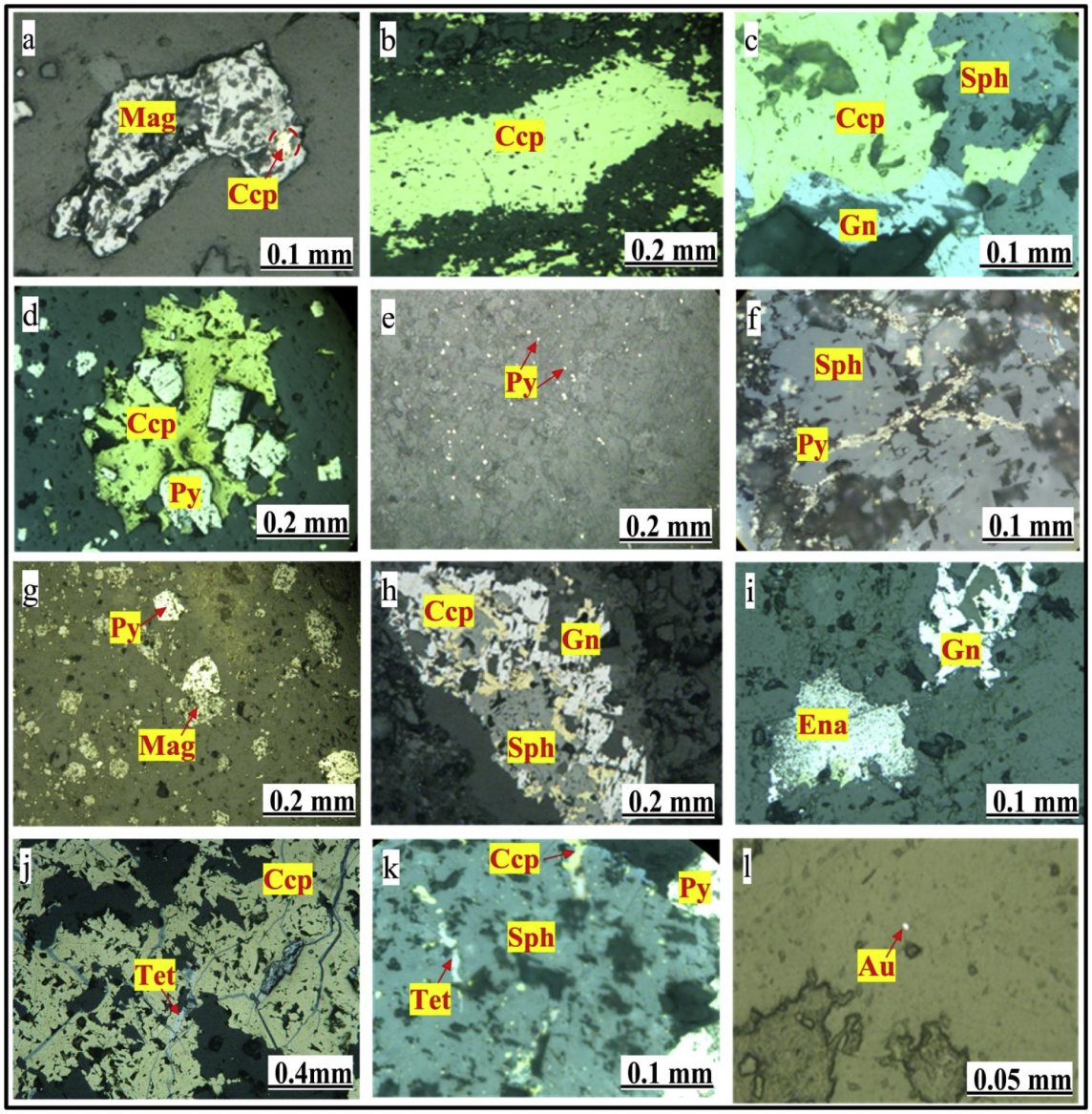

Fig. 9. Ore minerals in plane-polarized reflected light: (a) Disseminated chalcopyrite and magnetite in the deepest part of the intrusion; (b) Veinlet chalcopyrite; (c) Simple grain boundary relationships between chalcopyrite, galena, and sphalerite; extremely fine-grained inclusions of chalcopyrite (yellow) are present in the sphalerite (chalcopyrite disease); (d) Pyrite surrounded by chalcopyrite; (e) Very-fine disseminated pyrite (pyrite II generation); (f) Pyrite III is associated with sphalerite; (g) Rounded disseminated pyrite IV and disseminated magnetite; (h) Chalcopyrite, galena and sphalerite; galena surrounded sphalerite; (i) Enargite and galena; (j) Tennantite inclusion in chalcopyrite; (k) Tennantite and chalcopyrite veinlets in sphalerite associated with pyrite; (l) Gold and darker quartz gangue. Abbreviations: Ccp: Chalcopyrite, Py: Pyrite; Sph: Sphalerite; Gn: Galena; Ena: Enargite; Tet: Tennantite; Mag: Magnetite; Au: Gold. (For interpretation of the references to colour in this figure legend, the reader is referred to the web version of this article.)

dominant, halite and in some places, sylvite and opaque minerals (hematite and chalcopyrite) exist as daughter crystals. Halite occupies 20–40% of the volume and is cubic and lesser as sphere form. The vapor occupies 20–30% of the volume. The inclusions are 5–40 μm (Fig. 16e).

Type VI is oval, square and irregular and includes CO_2 as liquid and vapor in addition to another liquid phase (three-phase). They are 10–30 μm (Fig. 16f).

5.7.1.2. Fluid inclusion types in the sphalerite. Light-colored sphalerite is a rare case of sulfides, which can be studied using the optical microscopy for fluid inclusions and has two types of fluid inclusions (Fig. 17a–c).

Type II is oval, and vapor occupies more than 90% of the volume. It is between 5 and 30 μm (Fig. 17a and b).

Type III has oval, sphere and cylinder shapes, is 5–10 μm. The vapor occupies ~30% of the volume (Fig. 17c).

5.7.1.3. Types of fluid inclusions in the biotite. One single type is hosted by biotite at a depth of ~59 m.

Type III forms a negative crystal. Its average length is ~15 μm. The vapor occupies more than 90% of the volume (Fig. 17d).

5.7.1.4. Types of fluid inclusions in the plagioclase. Vapor only and two-phase (liquid-rich) fluid inclusions are hosted by plagioclase (Fig. 17e–f).

Type I has an average length of ~25 μm. Inclusion shapes are cylinderal and some spread in the plagioclases (Fig. 17e). Mostly trails arranging of fluid inclusions in cleavages give evidence of pseudo-secondary origin.

Type II appears at the center of the plagioclases as cylinder and irregular. The vapor occupies ~30% of the volume (Fig. 17f).

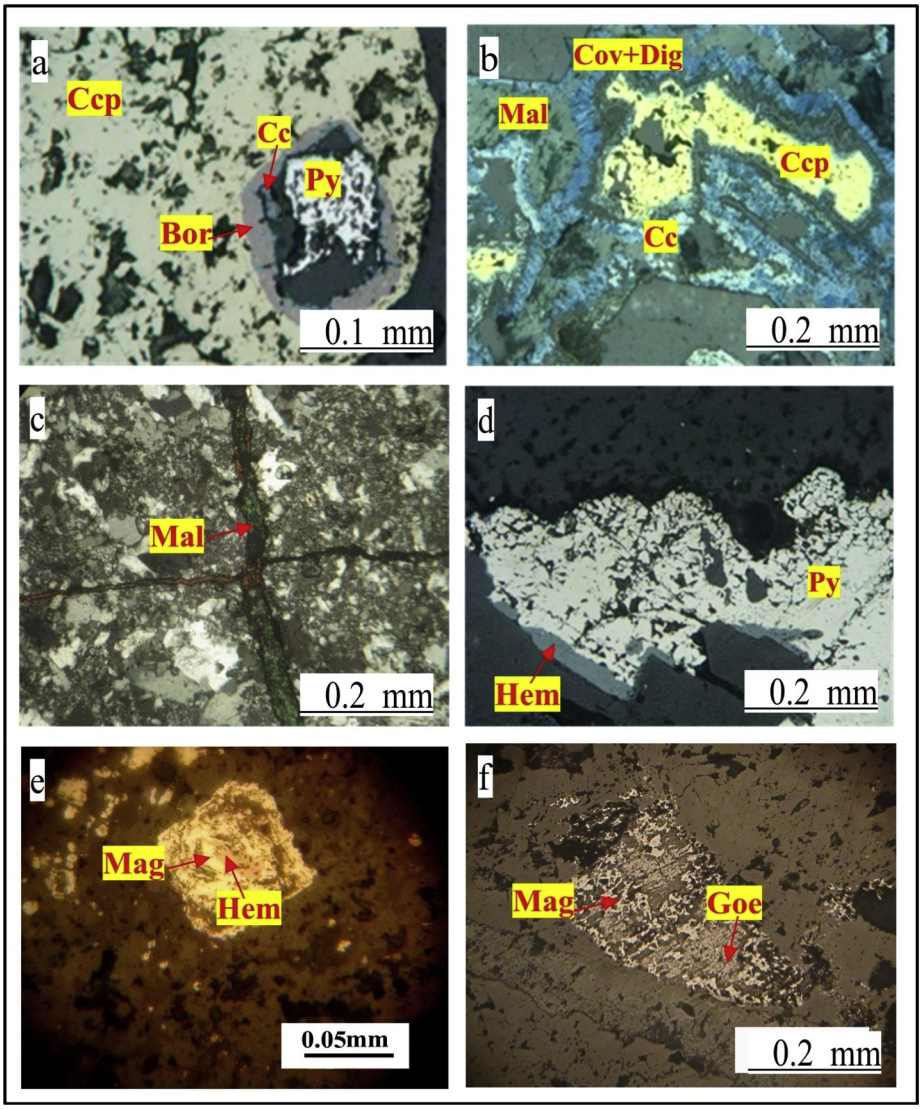

Fig. 10. (a) Pyrite enclosed by chalcopyrite; replacement relationships between chalcopyrite, chalcocite, and bornite; (b) Replacement relationships between chalcopyrite, chalcocite, malachite and blue copper sulfides (largely covellite and digenite); (c) Malachite veinlet; (d) Pyrite replaced by hematite; (e) Hematite replacing magnetite; (f) Goethite replacing magnetite. Abbreviations: Ccp: Chalcopyrite; Cc: Chalcocite; Cov: Covellite; Dig: Digenite; Bor: Bornite; Py: Pyrite; Mag: Magnetite; Hem: Hematite; Goe: Goethite. (For interpretation of the references to colour in this figure legend, the reader is referred to the web version of this article.)

5.7.2. Daughter minerals

The incident of daughter minerals over a wide area has been reported in porphyry systems (Wilkinson, 2001). The most distinguishing feature of the Chodarchay is the common occurrence of highly saline inclusions containing multiple daughter minerals including halite, sylvite and commonly chalcopyrite (Fig. 18a–c). These often coexist with low-density vapor inclusions (Fig. 18a); hence the assemblages are commonly interpreted as the product of liquid-vapor phase separation, a process considered to be an intrinsic part of the magmatic–hydrothermal evolution of such systems (Henley and McNabb, 1978). The common occurrence of chalcopyrite and hematite in magmatic-related inclusions (Fig. 18a, d–f) testifies to the high levels of dissolved Fe in such fluids. Recent data indicate that Fe is a major component of such solutions, together with K, Na and lesser amounts of Ca (Rankin et al., 1992; Wilkinson et al., 1994; Ulrich et al., 1999).

Chalcopyrite as opaque and triangular (Fig. 18a) indicates to Cu-rich fluids. Copper was transported by fluids from the magma to a higher level into the Cu mineralization area. Both brine and vapor-rich inclusions are ubiquitous in porphyry deposits, and the presence of chalcopyrite in either inclusion type in various deposits implicates both fluid phases as efficient Cu-transporting mediums (Ulrich et al., 2001; Bouzari and Clark, 2006). Chalcopyrite-bearing inclusions are trapped in quartz crystals containing small chalcopyrite crystals and suggest that crystals host fluids that precipitated chalcopyrite at depth. These inclusions commonly contain liquid, vapor bubble and halite (Fig. 18a). These oval and sometimes irregular inclusions contain opaque and/or transparent daughter minerals, and a few contain up to three daughter minerals.

5.7.3. Necking

Large and irregular inclusions by splitting into several smaller, more equant inclusions in a post-entrapment process tend towards morphological equilibrium and minimization of surface free-energy. During this process, the asperities in the inclusion walls narrow down, adopting shapes that resemble necks. This subsequent event has occurred in the fluid inclusions of the Chodarchay samples (Fig. 19), so it has been considered in the petrography of the fluid inclusions.

5.7.4. Boiling and flashing

In many ore deposits, physical processes are the most important mechanisms that result in the deposition of economic concentrations of ore minerals (e.g., Skinner, 1997). The two processes that commonly

	Time →						
	Mineralization						
	Porphyry mineralization		Epithermal mineralization			Supergene	
Minerals	Stage 1	Stage 2	Stage 1	Stage 2	Stage 3	Stage 1	Stage 2
Magnetite	—			—	—		
Hematite (Specularite)			—				
Pyrite	—	—	—	—	—		
Chalcopyrite	—		—	—			
Sphalerite		—		—			
Galena		—		—			
Tetrahedrite-Tennantite				—			
Enargite				—			
Gold				—			
Bornite				—	—		
Chalcocite				—	— - - -	—	
Covellite				—	— - - -	—	
Digenite				—	— - - -	—	
Malachite							—
Azurite							—
Iron oxide							—

Fig. 11. Paragenetic sequence for porphyry and epithermal mineralization types from the Chodarchay deposit.

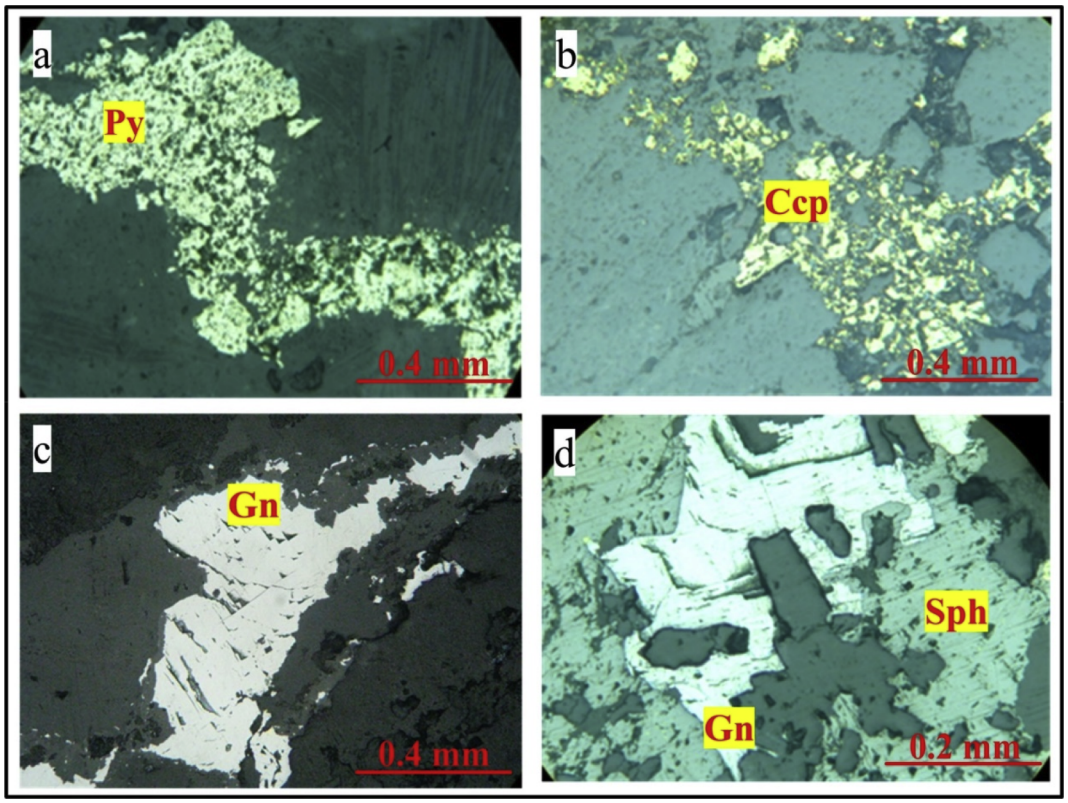

Fig. 12. Some ore minerals at the Chodarchay display post-mineral tectonic event: (a) Brecciated pyrite; (b) Crackle brecciated chalcopyrite; (c–d) Galena cleavages (triangular pits) elongation. Note elongated cleavage pits. (c) Galena. (d) Galena plus sphalerite. Abbreviations: Py: Pyrite; Ccp: Chalcopyrite; Gn: Galena; Sph: Sphalerite.

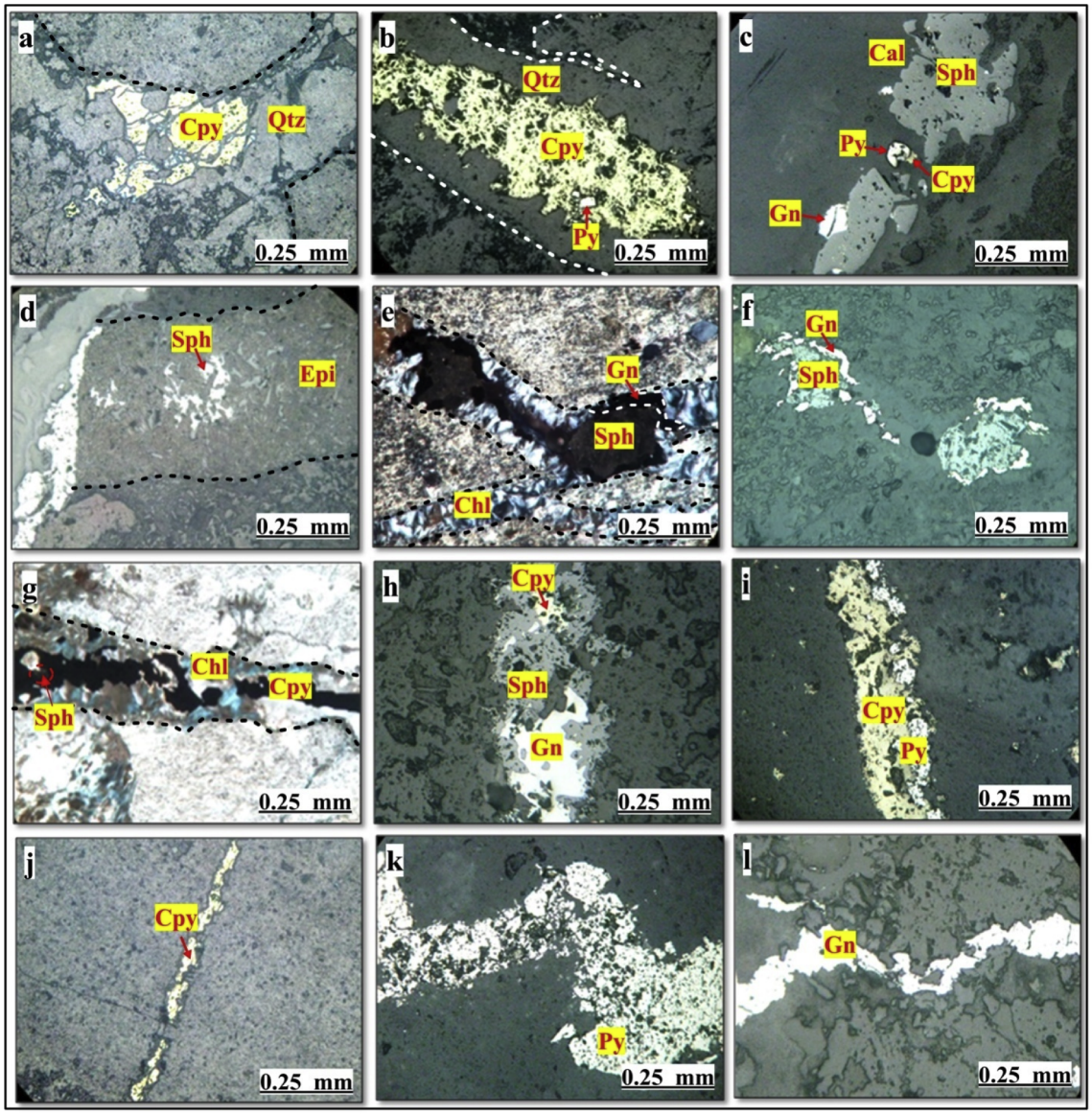

Fig. 13. Microscopic images of various types of hydrothermal veinlets at the Chodarchay deposit: (a) Quartz-chalcopyrite veinlet; (b) Quartz-chalcopyrite-pyrite veinlet; (c) Calcite-sphalerite-galena-pyrite-chalcopyrite veinlet; (d) Epidote-sphalerite veinlet; (e-f) Chlorite-sphalerite-galena veinlet in cross-polarized light and plane-polarized reflected light; (g) Chlorite-chalcopyrite-sphalerite veinlet; (h) Galena-sphalerite-chalcopyrite-pyrite veinlet; (i) Chalcopyrite-pyrite veinlet; (j) Chalcopyrite veinlet; (k) Pyrite veinlet; (l) Galena veinlet.

provide the necessary conditions for effective ore mineral precipitation are boiling, or effervescence in volatile-rich systems, and fluid mixing (Wilkinson, 2001).

Coexistence of the types II and III fluid inclusions can indicate fluid boiling at the time of entrapment. Vapor-rich inclusions that result from boiling in low depth and pressure are predominant in near-surface environment. In systems containing volatiles such as CO_2, using the term effervescence is more proper than boiling. The partitioning of vapor from a more saline residual liquid can occur by boiling or effervescence (Wilkinson, 2001).

If pressure decreases to less than hydrostatic pressure leads to 100% of the original liquid convert into a low-density vapor, boiling is referred to as flashing (Moncada et al., 2012). Boiling or effervescence and flashing can be concluded from petrography of the Chodarchay fluid inclusions. There is strong textural and fluid inclusion evidence that boiling was widespread during the mineralizing events. Fluid inclusion characteristics of fluid immiscibility or boiling including coexisting liquid-rich and vapor-rich inclusions and assemblages of vapor-rich only inclusions (flashing) have been identified in the mineralized samples (Fig. 20).

6. Discussion

Mineralization in the high-sulfidation epithermal environment appears to be genetically linked to deeper porphyry deposits (e.g., Arribas et al., 1995; Hedenquist et al., 1998; Einaudi et al., 2003; Pudack et al., 2009). The development of a high-sulfidation deposit is related to fluid evolution in the underlying porphyry. Mineralization at the Chodarchay commenced as a porphyry system that evolved to epithermal conditions.

Porphyry mineralization is related to the emplacement of the quartz monzonite plutonic body that intruded into the Karaj Formation. Phyllic and argillic alterations overprint earlier potassic alteration. The overprinting of potassic alteration by phyllic alteration has been widely reported in porphyry copper systems (Landtwing et al., 2010; Sillitoe, 2010), and this alteration paragenetic sequence is characteristic of most

Table 2
Distribution of hydrothermal veinlet types from the surface to the depth associated with their host rocks and related hydrothermal alteration. Abbreviations: Qtz: Quartz; Cal: Calcite; Epi: Epidote; Cpy: Chalcopyrite; Py: Pyrite; Sph: Sphalerite; Gn: Galena.

Sample No.	Depth (m)	Lithology	Alteration type	Veinlet type
001-1	0.2	Rhyolitic tuff	Tourmaline-siliceous	Qtz – Py
1-1	7.2	Hydrothermal breccia	Tourmaline-siliceous	Qtz – Py – Cpy
1-2	7.5	Hydrothermal breccia	Tourmaline-siliceous	Qtz - Py – Cpy
1-4	10.7	Breccia	Tourmaline-siliceous	Cpy; Qtz – Cpy
9-3	18	Alkali granite	Argillic	Py, Cpy; Sph – Cpy
5-3	20	Siliceous vein	Siliceous	Py
22-1	24.2	Alkali granite	Intermediate argillic-carbonated	Chl – Cpy – Sph
17-8	25.2	Breccia	Phyllic-tourmaline	Cpy
12-1	26	Breccia	Argillic	Cpy – Gn – Sph, Py; Qtz – Cpy – Py
1-8	30.3	Rhyolitic tuff	–	Qtz – Sph – Cpy – Gn
1-9	31.7	Rhyolitic crystal tuff	Siliceous-carbonated	Qtz – Sph – Cpy
10-5	32.8	Rhyolite	Phyllic-carbonated	Cpy – Gn – Sph; Qtz – Cpy
9-5	33	Alkali granite	Phyllic	Cpy – Gn – Sph
20-2	34.3	Breccia	Siliceous-carbonated-tourmaline	Qtz – Cpy – Py
5-4*	35	Volcanic	Siliceous	Cpy – Py; Cpy
15-11	35	Breccia	Siliceous-carbonated	Cpy – Py
5-8	40.3	Rhyolitic tuff	Siliceous	Cpy – Gn – Sph, Cpy
3-1	41.6	Rhyolitic crystal tuff	Carbonated	Gn – Py
9-6	53.8	Alkali granite	Argillic	Cpy – Gn – Sph, Gn
1-12	59.3	Alkali granite	Argillic	Qtz – Py – Cpy
11-4	61.20	Rhyolitic lithic-crystal tuff	Phyllic-carbonated	Qtz – Cpy – py
15-14	61.3	Trachyte	Propylitic	Cal – Cpy – Gn – Sph; Epi – sph
15-18	66.5	Alkali granite	Propylitic	Epi – Sph – Cpy – Py – Gn
1-16	89.4	Alkali granite	Phyllic-carbonated	Py – Sph

porphyry deposits hosted in intermediate rocks. The occurrence of enargite suggests that some portion of the high-sulfidation epithermal system has been preserved and was not destroyed by supergene processes, as has been recognized in some other porphyry deposits by Sillitoe (2005).

High salinity inclusions recognized by fluid inclusion petrography and daughter minerals (halite and sylvite) are closely associated with the porphyry system. Fluid inclusions in epithermal systems are typified by low salinity fluids (Wilkinson, 2001). Detected daughter minerals in the Chodarchay samples are commonly observed in typical porphyry systems (Wilkinson, 2001). In the porphyry systems, the occurrence of hypersaline fluid inclusions containing several daughter minerals and/or vapor-rich inclusions has been linked to ore (Roedder, 1971; Nash, 1976; Bodnar, 1981). Vapor-rich inclusions are seen in shallow porphyry systems (Bodnar, 1982; Hedenquist et al., 1998; Muntean and Einaudi, 2000) and precious metal epithermal systems (Buchanan, 1979; Moncada et al., 2012). They represent the fluids responsible for advanced argillic alteration. Solids nucleation from an oversaturated liquid solution has been indicated by the presence of daughter minerals. Na^+, Cl^-, K^+, Cu^{2+}, and Fe^{2+} in these hypersaline fluids are the most common dissolved ions. The abundance of NaCl in fluid inclusions in hydrothermal systems points out to the significance of chloride complexing. $ZnCl_2$, $CuCl_2$ and $AgCl_2$ aqueous species can form in chloride-rich solutions. Chloride complexes are more stable than sulfide complexes at higher temperatures (above 350 °C; Barnes, 1979). This complexing can be valid for the transport of Au in the deeper and hotter parts of magmatic and hydrothermal systems. Deeper than 24 m, all samples have type V (hypersaline fluids), but in shallow levels, the halite-bearing inclusions decrease. Lower salinity in shallower depths can reflect dilution by meteoric waters. Therefore, the second mechanism has been effective at the Chodarchay mineralization system. During the epithermal stage, the salinity of aqueous fluid was lower. It may be because of low salinity magmatic vapor transfer to near surface. More saline liquid has stayed at depth (Henley and McNabb, 1978). In many porphyry systems, potassic alteration forming at temperatures above approximately 450 °C is associated with quartz veins containing these hypersaline liquid inclusions (e.g., Redmond et al., 2004; Williams-Jones and Heinrich, 2005).

Homogeneous hydrothermal fluids exsolved from deep to moderately deep intrusions undergo phase separation to a low salinity vapor and a corresponding hypersaline liquid during ascent and cooling (Hedenquist et al., 1998). The relatively low buoyancy of the hypersaline liquid causes it to remain at depth, where it generates potassic alteration in the porphyry environment (Heinrich, 2005). According to Arribas (1995), the rising low salinity vapors to shallow crustal levels interact with meteoric water and generate the acid-type alteration that characterizes epithermal deposits that exist at the Chodarchay.

Fluid inclusion association, including vapor-, liquid-rich two-phase, opaque mineral or unknown transparent mineral-bearing inclusion, halite with or without sylvite and hematite-bearing inclusion and minor CO_2-bearing fluid inclusions at the Chodarchay, resemble those commonly observed in typical porphyry systems in the world (Lu et al., 2004; Chen et al., 2007; Pirajno, 2009). There is a strong correlation between CO_2 content and gold mineralization, such as in the deep-seated intrusion-related systems (Lowenstern, 2001; Baker, 2002).

Even where the genetic relationship between porphyry and epithermal mineralization is evident, physical and chemical evolution of hydrothermal systems that accompany this transfer, need further investigation (Gammons and Williams-Jones, 1997; Muntean and Einaudi, 2001; Sillitoe and Hedenquist, 2003; Heinrich et al., 2004). Deposit-scale distribution of fluid inclusions shows that fluid inclusions evolved spatially and temporally during the life of the hydrothermal system from porphyry to epithermal type. Coexisting vapor- and liquid-rich inclusions are observed in the upper part of the system indicating that boiling occurred. The coexistence of the types II and III fluid inclusions is characteristic of porphyry copper systems (Bodnar, 1995; Roedder and Bodnar, 1997). In epithermal systems, the occurrence of cogenetic vapor- and liquid-rich inclusions may be used to identify zones of boiling or immiscibility and ore mineral precipitation (Kamilli and Ohmoto, 1977). Type IV at shallower levels emphasizes flashing of hydrothermal fluids. Flashing is the result of fractures and pressure decrease; so flashing at the Chodarchay can support the structural control. Type VI near the surface indicates to the effervescence or immiscibility. Fluid immiscibility emphasized by fluid inclusion evidence, is characteristic of porphyry copper deposits (Roedder, 1971; Nash, 1976; Roedder, 1984; Bodnar, 1995), and by the partitioning of metals

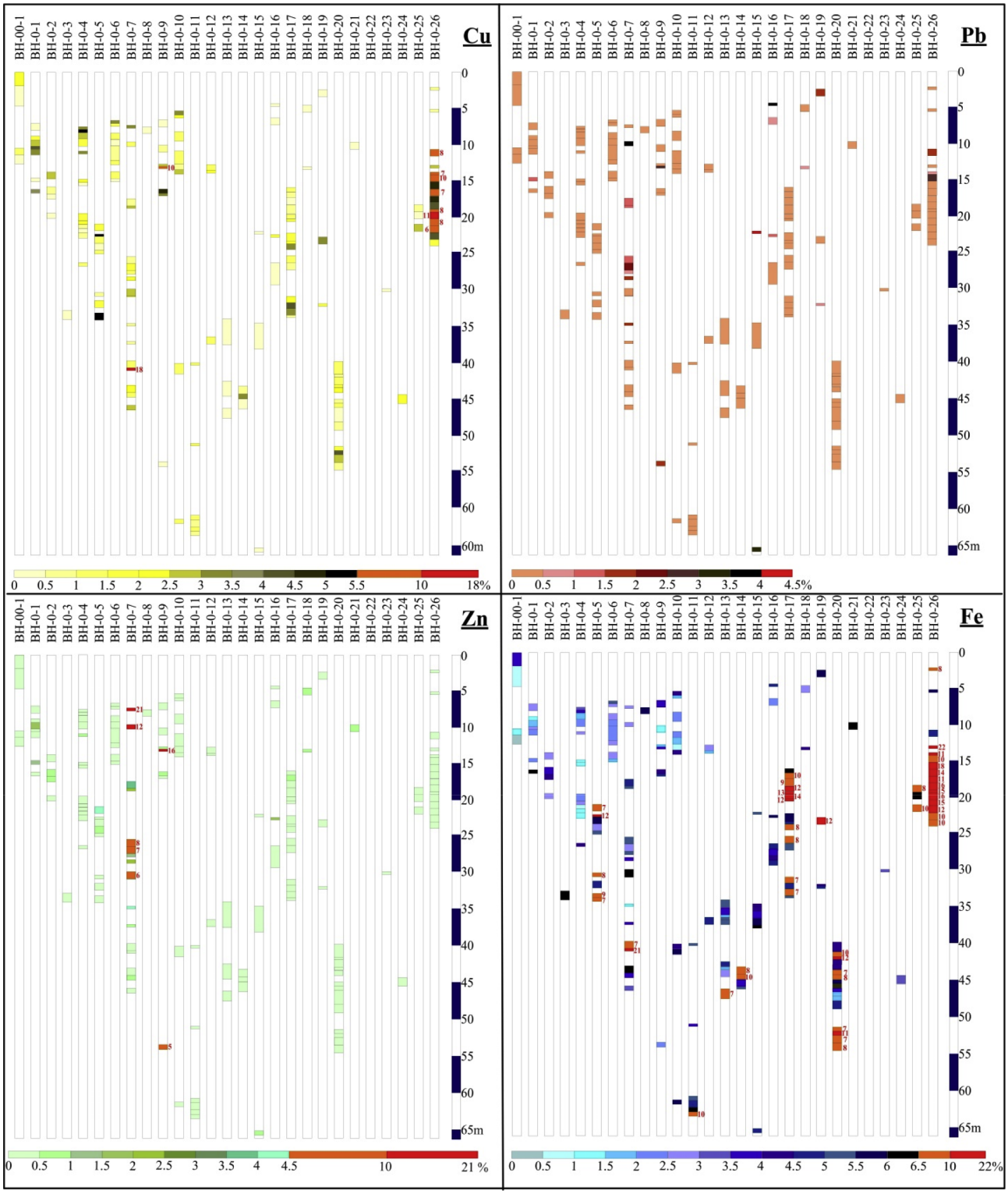

Fig. 14. Variation in the grades of ore-related metals including Cu (a), Pb (b), Zn (c) and Fe (d) with depth at the Chodarchay deposit.

and other species between vapor and hypersaline liquid may result in metal and sulfide zoning patterns in porphyry deposits (Heinrich et al., 1999; Audétat et al., 2000). Type V and salinity changes provide evidence for the fluids flow and salinity decrease from the porphyry upwards to the high-sulfidation system with focusing on boiling, flashing and faulting.

Schematic genetic section of the Chodarchay indicating fluid inclusion distribution as well as veinlet types are illustrated in Fig. 21 based on field mapping, core logging, and microscopic examinations. The Chodarchay formed in relation to high-level volatile-rich quartz monzonite. The porphyry mineralization is typically associated with saline fluids in the quartz monzonite. Continuation of crystallization led

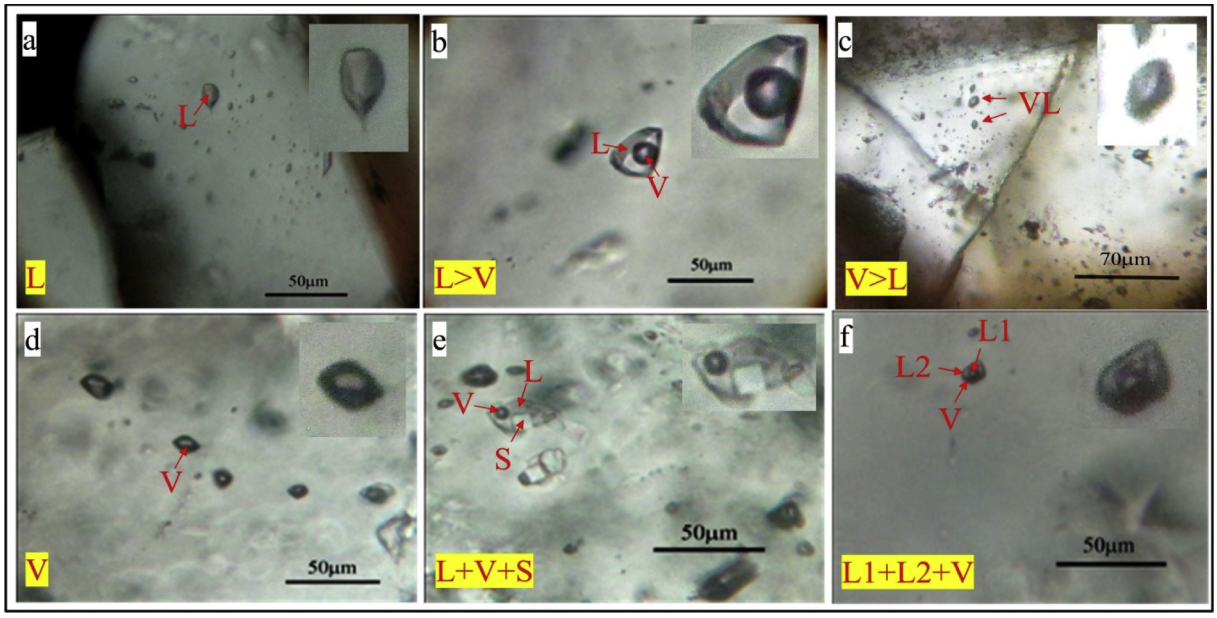

Fig. 15. Six fluid inclusion types at the Chodarchay deposit: (a) Type I: Liquid monophase; (b) Type II: Liquid > 50% + Vapor < 50%; (c) Type III: Vapor > 50% + Liquid < 50%; (d) Type IV: Vapor only; (e) Type V: Liquid ± Vapor + Solid (> 50% or < 50%); (f) Type VI: Immiscible Liquid L_1 + L_2 ± Vapor. V: Vapor; L: Liquid; S: Solid.

Table 3
Fluid inclusion types in host minerals at the Chodarchay epithermal-porphyry deposit. H: Halite; S: Sylvite; He: Hematite; O.m.: Opaque mineral; T.m.: Transparent mineral; Cpy: Chalcopyrite.

Sample No.	Lithologic unit	Depth (m)	Fluid type in				Daughter minerals
			plagioclase	biotite	sphalerite	quartz	
*CHO6**	***Late alkali granite***	***0***	**–**	**–**	**–**	***II, III, V***	***H, S, O.m., T.m.***
CHO24	Quartz monzonite	0	–	–	–	II, III, V	H
CHO36	Tuff	0	–	–	–	II	–
CHO44	Quartz monzonite	0	–	–	–	II, III, V	H
001-1	Tuff	0.2	–	–	–	II, V	H
19-2	Early alkali granite	4.4	–	–	–	II, III, IV, V	H
18-2	Quartz syenite	6.2	–	–	–	II	–
25-1	Early alkali granite	10.9	–	–	–	II, VI	–
17-2	Early alkali granite	14	–	–	–	I, II, III	–
22-1	Early alkali granite	24.2	–	–	–	II	–
18-6	Quartz monzonite	26	I, II	–	–	II, III, IV, V	H, O.m., T.m.
20-2	Volcanic	34.3	–	–	–	II, V	H, He, T.m.
15-11	Breccia	35	–	–	–	II, V	H, O.m.
04-5	Early alkali granite	36.5	–	–	–	II, IV, V	H
03-1	Tuff	41.6	–	–	–	II, IV, V	H
24-6	Early alkali granite	43.3	–	–	–	II, III, IV, V	H, O.m. T.m.
24-7	Quartz monzonite	59.1	I	III	–	II, III, V	H
01-12	Early alkali granite	59.3	–	–	II, III	II, III, V	H, S, O.m., T.m.
15-14	Volcanic	61.3	–	–	–	II, III, IV. V	H, He, Cpy, T.m.
14-7	Breccia	97.3	–	–	–	II, III, V	H

* Late alkali granite outcropped at the surface is aside from the quartz monzonite series.

to increasing fluid pressure and fracturing. Hydrothermal mineral deposition closed these hydrothermal and tectonic open spaces, so fluid pressure increased resulting in fracturing and secondary boiling event. The presence of the extensive hydrothermal brecciation within the ore zones show the possibility of boiling. As a result of the exit of acidic fluids, vuggy quartz formed in the epithermal environment. Fluids became progressively neutralized, cooler and low-salinity outward by fluid-rock interaction and meteoric water dilution. High-sulfidation epithermal mineralization formed during these processes overprinting the early deeper-seated porphyry mineralization at the Chodarchay.

7. Conclusions

Field evidence, core logging, prevailing mineralogical and geochemical data along with other data obtained from the Chodarchay indicate two stages of ore formation. The Chodarchay is the only

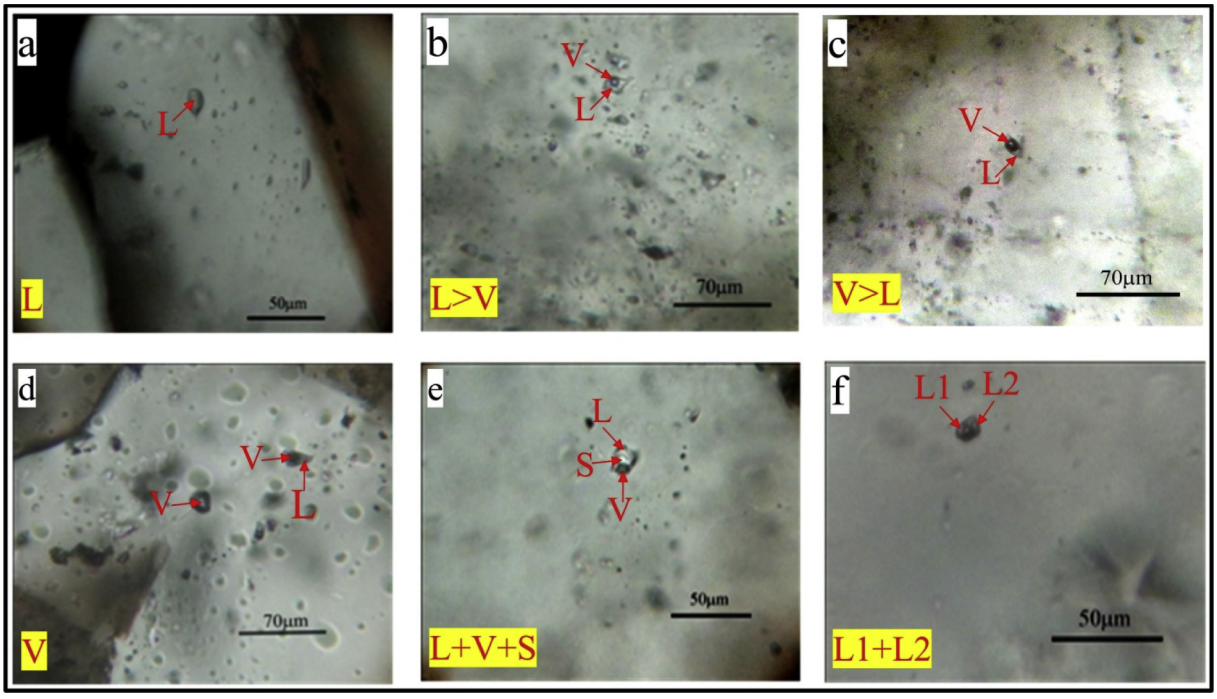

Fig. 16. Six types of fluid inclusions were recognized in the quartz crystals from the Chodarchay deposit. (a) Type I, (b) Type II, (c) Type III, (d) Type IV, (e) Type V, (f) Type VI. V: Vapor; L: Liquid; S: Solid.

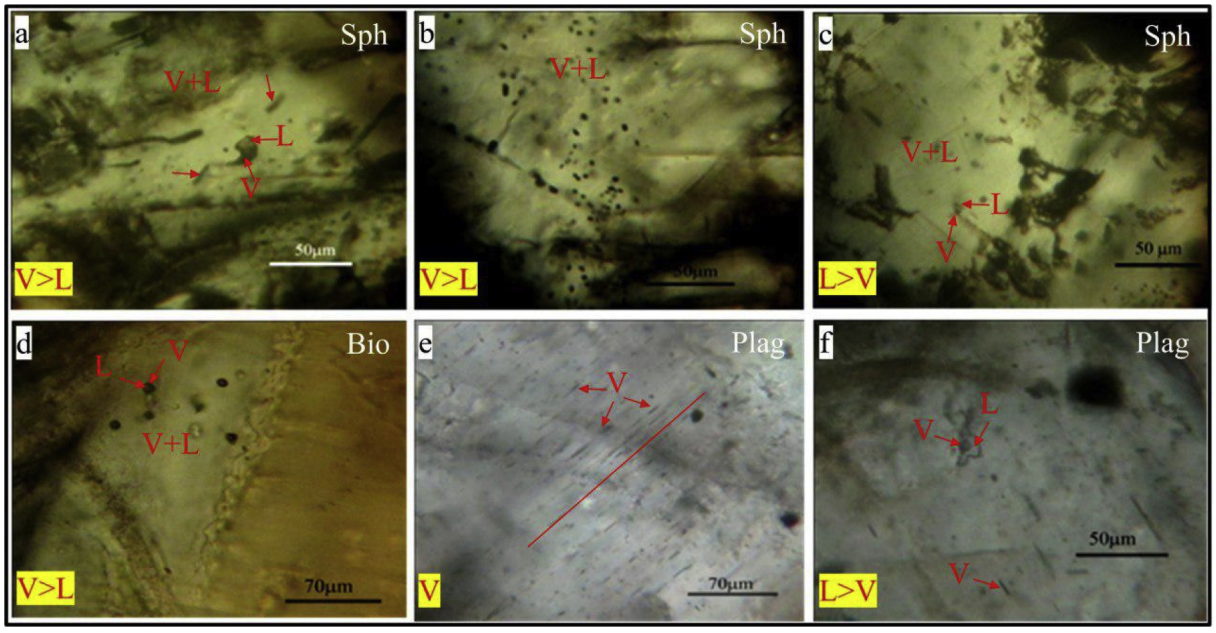

Fig. 17. Microphotographs showing different types of fluid inclusions observed in sphalerite, plagioclase and biotite at the Chodarchay deposit. (a–b) Type II fluid inclusion in the sphalerite. (c) Type III fluid inclusion in the sphalerite. (d) Type III fluid inclusion in the biotite. (e) Type I fluid inclusion in the plagioclase. (f) Types I and II fluid inclusions in the plagioclase. Sph: Sphalerite; Bio: Biotite; Plag: Plagioclase; V: Vapor; L: Liquid.

example of a spatial association and transition of porphyry to high-sulfidation epithermal systems in the Tarom subzone of western Alborz structural zone of northwestern Iran. Both epithermal and porphyry systems have been preserved. Mineralization is hosted in the quartz monzonite and the surrounding volcanic and volcaniclastic units.

The fluid inclusion distribution and paragenetic sequence indicate that a magmatic fluid at depth evolved with time from a high-salinity to a low-salinity mineralizing fluid and hydrothermal ores precipitated from fluids with variable salinities. Boiling was a dominant process at shallow levels in the system.

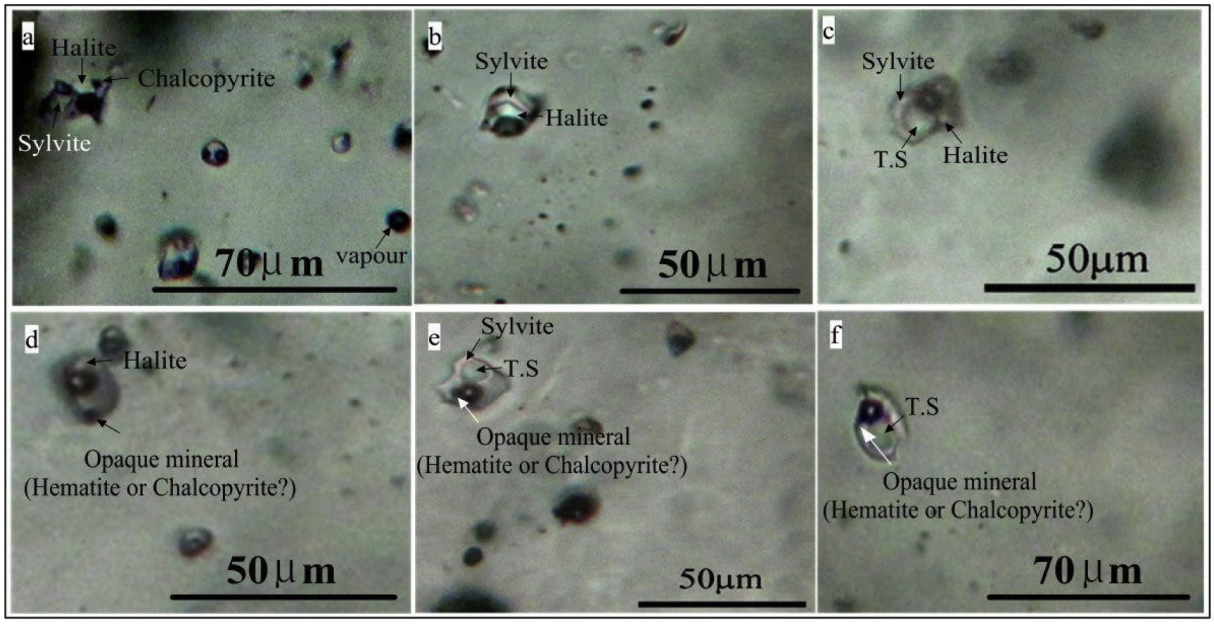

Fig. 18. Daughter minerals in fluid inclusions from the Chodarchay deposit. (a) Multiple daughter minerals including halite, sylvite and triangular chalcopyrite associated with vapor inclusion. (b) Multiple daughter minerals including sylvite and halite. (c) Multiple daughter minerals including halite, sylvite, and transparent solid phase. (d) Halite and opaque mineral (hematite or chalcopyrite) as daughter minerals. (e) Sylvite, opaque mineral (hematite or chalcopyrite) and transparent solid phase as daughter minerals. (f) Opaque mineral (hematite or chalcopyrite) and transparent solid phase as daughter minerals. T.S: Transparent Solid phase.

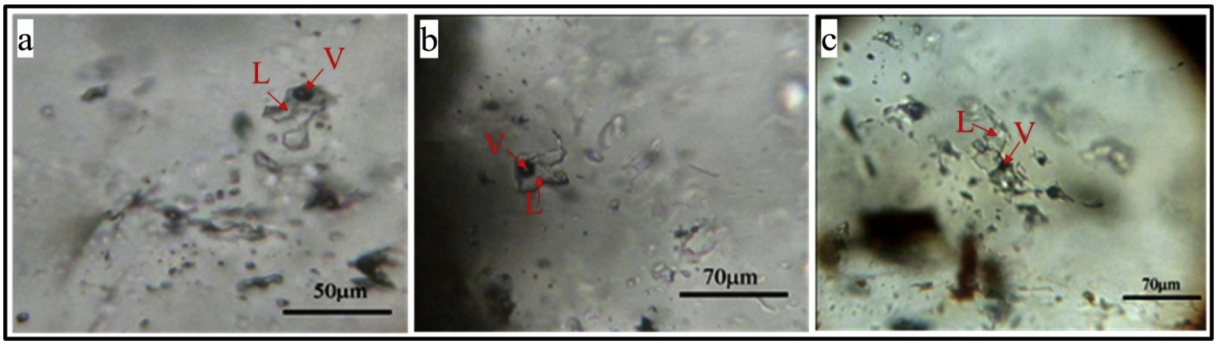

Fig. 19. (a–c) Fluid inclusion necking observed in transmitted light from the Chodarchay samples shows changes after trapping. V: Vapor; L: Liquid.

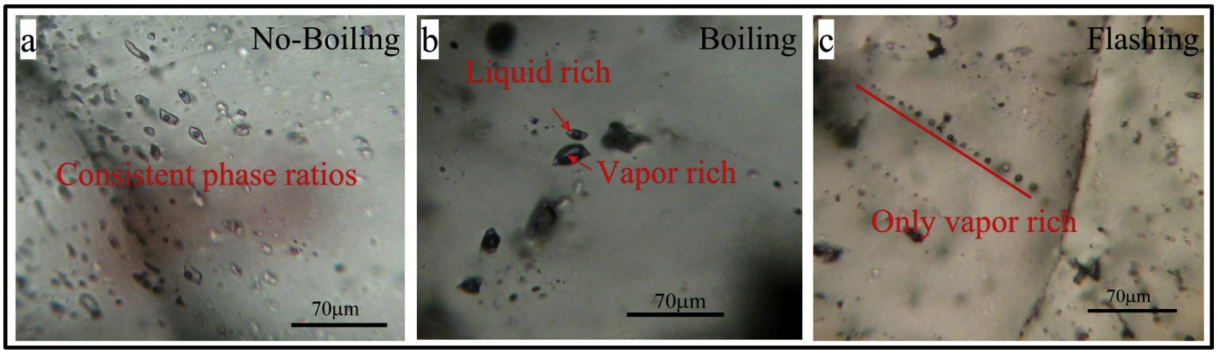

Fig. 20. Fluid inclusion types observed in samples from the Chodarchay: (a) Fluid inclusion assemblages (FIAs) containing liquid-rich inclusions only with consistent liquid-to-vapor ratios are indicative of non-boiling conditions. (b) FIAs consisting of coexisting liquid-rich and vapor-rich inclusions are indicative of boiling conditions. (c) FIAs containing only vapor-rich inclusions indicate flashing of the system.

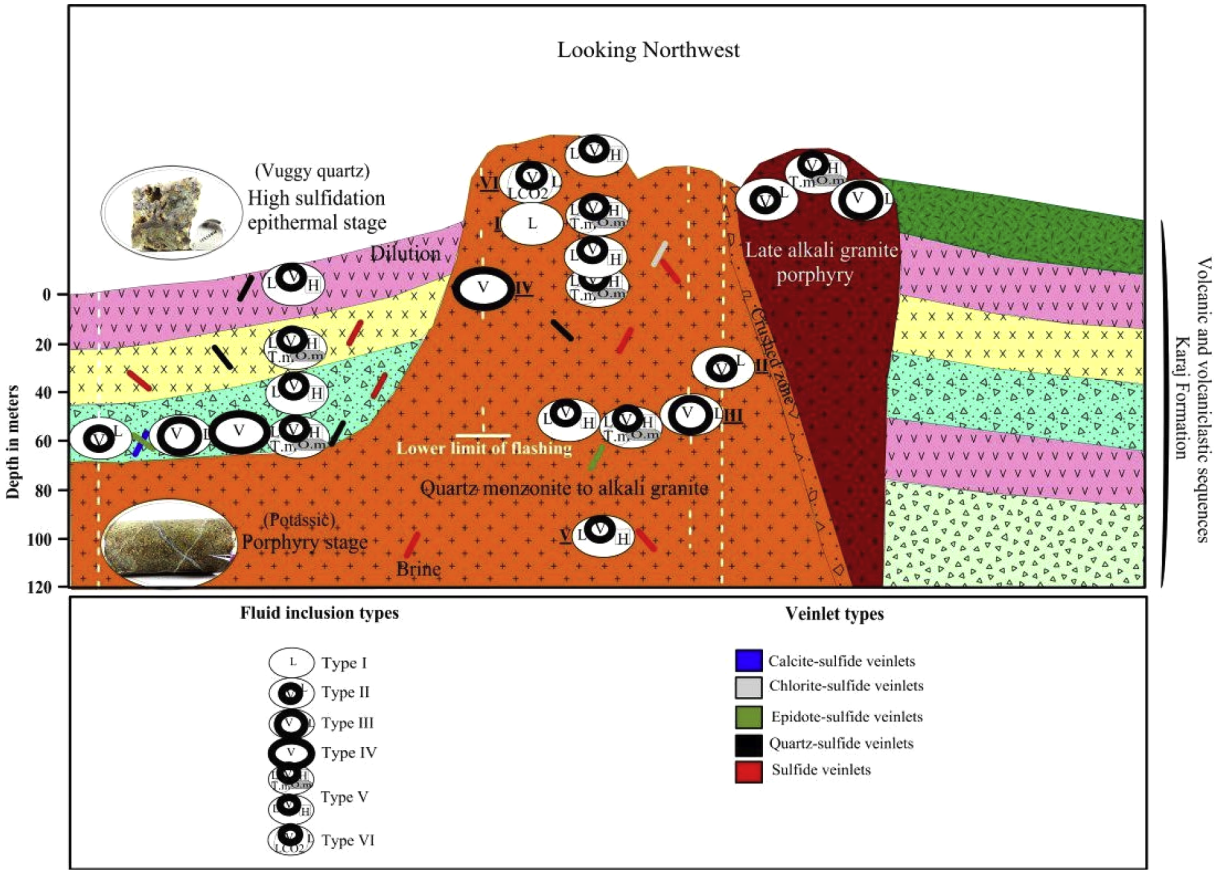

Fig. 21. Deposit-scale distribution of fluid inclusions and veinlet types at the Chodarchay deposit.

The distribution of alteration, mineralization, and fluid inclusion features at Chodarchay provides vectors that show systematic variations from depth to surface in porphyry–epithermal systems.

Acknowledgments

This paper represents a part of the first author's Ph.D. thesis at Tarbiat Modares University, Tehran, Iran. Appreciation is extended to Madankaran Angouran Company for generously providing field survey facilities and access to drill cores and exploration data. We would like to thank Nematollah Rashidnejad-Omran and Hossein-Ali Tajeddin for their constructive reviews on the manuscript. Franco Pirajno and Hooshang Asadi Haroni are also thanked for careful editorial handling of the manuscript.

References

Aghazadeh, M., Castro, A., Omran, N.R., Emami, M.H., Moinvaziri, H., Badrzadeh, Z., 2010. The gabbro (shoshonitic)–monzonite–granodiorite association of Khankandi pluton, Alborz mountains, NW Iran. J. Asian Earth Sci. 38, 199–219. https://doi.org/10.1016/j.jseaes.2010.01.002.

Albinson, T., Norman, D.I., Cole, D., Chomiak, B., 2001. Controls on formation of low-sulfidation epithermal deposits in Mexico: constraints from fluid inclusion and stable isotope data. SEG Spec. Publ. 8, 1–32.

Arribas Jr., A., 1995. Characteristics of high-sulfidation epithermal deposits, and their relation to magmatic fluid. Mineral. Assoc. Canada Short Course 23, 419–454.

Arribas Jr., A., Hedenquist, J.W., Itaya, T., Okada, T., Concepcion, R.A., Garcia Jr., J.S., 1995. Contemporaneous formation of adjacent porphyry and epithermal Cu-Au deposits over 300 ka in northern Luzon, Philippines. Geology 23, 337–340.

Audétat, A., Gunther, D., Heinrich, C.A., 2000. Magmatic-hydrothermal evolution in a fractionating granite: A microchemical study of the Sn-W-F mineralized Mole granite, Australia. Geochim. Cosmochim. Acta 64, 3373–3393. https://doi.org/10.1016/S0016-7037(00)00428-2.

Baker, T., 2002. Emplacement depth and carbon dioxide-rich fluid inclusions in intrusion-related gold deposits. Econ. Geol. 97, 1111–1117. https://doi.org/10.2113/97.5.1111.

Barnes, H.L., 1979. Solubilities of ore minerals. In: Barnes, H.L. (Ed.), Geochemistry of Hydrothermal Ore Deposits. John Wiley, New York, pp. 971.

Berberian, F., Berberian, M., 1981. Tectono-plutonic episodes in Iran. In: Gupta, H.K., Delany, F.M. (Eds.), Zagros Hindukush Himalaya Geodynamic Evolution. American Geophysical Union, Washington, DC, pp. 5–32.

Berberian, M., King, G.C.P., 1981. Towards a paleogeography and tectonic evolution of Iran. Can. J. Earth Sci. 18, 210–265.

Birch, W.D., Primc, A., Reller, A., Schmalle, H.W., 1992. Bernalite: a new ferric hydroxide with perovskite structure. Naturwiss 79, 509–511.

Birch, W.D., Princ, A., Reller, A., Schmalle, H.W., 1993. Bemalite, $Fe(OH)_3$, a new mineral from Broken Hill, New South Wales: description and structure. Am. Mineral. 78, 827–834.

Bodnar, R.J., 1981. Use of fluid inclusions in mineral exploration: comparison of observed features with theoretical and experimental data on ore genesis. Geol. Soc. Am. Abstr. Progr. 13, 412 p.

Bodnar, R.J., 1982. Fluid Inclusions in Porphyry-type Deposits. Course Notes, Mineral Deposits Research Review for Industry.

Bodnar, R.J., 1995. Fluid inclusion evidence of a magmatic source for metals in porphyry copper deposits. In: Thompson, J.F.H., ed., Magmas, Fluids and Ore Deposits. Mineral. Assoc. Canada Short Course 23, 139–152.

Bodnar, R.J., Reynolds, T.J., Kuehn, C.A., 1985. Fluid-inclusion systematics in epithermal systems. In: Berger, B.R., Bethke, P.M., eds., Geology and Geochemistry of Epithermal Systems. Reviews in Economic Geology 2, 73–97.

Bouzari, F., Clark, A.H., 2006. Prograde evolution and geothermal affinities of a major porphyry copper deposit: the Cerro Colorado hypogene protore, I Region, northern Chile. Econ. Geol. 101, 95–134. https://doi.org/10.2113/gsecongeo.101.1.95.

Brathwaite, R.L., Simpson, M.P., Faure, K., Skinner, D.N.B., 2001. Telescoped porphyry Cu-Mo-Au mineralisation, advanced argillic alteration and quartz-sulphide-gold-anhydrite veins in the Thames district, New Zealand. Miner. Deposita 36 (7), 623–640. https://doi.org/10.1007/s001260100182.

Brown, K.L., 1986. Gold deposition from geothermal discharges in New Zealand. Econ. Geol. 81 (4), 979–983.

Buchanan, L.J., 1979. The Las Torres Mines, Guanajuato, Mexico: Ore controls of a fossil geothermal system. Unpublished Ph.D. thesis, Colorado School of Mines, Golden, Colorado, 138 p.

Camprubí, A., Albinson, T., 2007. Epithermal deposits in Mexico–update of current knowledge, and an empirical reclassification. Geol. Soc. Am. Spec. Pap. 422, 377–415. https://doi.org/10.1130/2007.2422(14).

Castro, A., Aghazadeh, M., Badrzadeh, Z., Chirro, M., 2013. Late Eocene-Oligocene post-collisional monzonitic intrusions from the Alborz magmatic belt, NW Iran: an example of monzonite magma generation from a metasomatized mantle source. Lithos

180, 109–127.
Chen, Y.J., Ni, P., Fan, H.R., Pirajno, F., Lai, Y., Su, W.C., et al., 2007. Diagnostic fluid inclusions of different types of hydrothermal gold deposits. Acta Petrol. Sin. 23, 2085–2108 (in Chinese with English abstract).
Dilles, J.H., Einaudi, M.T., 1992. Wall-rock alteration and hydrothermal flow paths about the Ann Mason porphyry copper deposit, Nevada: a 6-km vertical reconstruction. Econ. Geol. 87, 1963–2001.
Einaudi, M.T., Hedenquist, J.W., Inan, E.E., 2003. Sulfidation state of fluids in active and extinct hydrothermal systems: transition from porphyry to epithermal environments. SEG Spec. Publ. 10, 285–314.
Gammons, C.H., Williams-Jones, A.E., 1997. Chemical mobility of gold in the porphyry-epithermal environment. Econ. Geol. 92, 45–59.
Goldstein, R.H., Reynolds, T.J., 1994. Systematics of fluid inclusions in diagenetic minerals. SEPM Short Course Notes 31, 199.
Hedenquist, J.W., Lowenstern, J.B., 1994. The role of magmas in the formation of hydrothermal ore deposits. Nature 370, 519–527. https://doi.org/10.1038/370519a0.
Hedenquist, J.W., Arribas, A., Reynolds, T.J., 1998. Evolution of an intrusion-centered hydrothermal system: Far Southeast-Lepanto porphyry and epithermal Cu–Audeposits, Philippines. Econ. Geol. 93, 373–404.
Hedenquist, J.W., Arribas, A., Gonzalez-Urien, E., 2000. Exploration for epithermal gold deposits. Rev. Econ. Geol. 13, 221–244.
Heinrich, C.A., 2005. The physical and chemical evolution of low- to medium salinity magmatic fluids at the porphyry to epithermal transition: a thermodynamic study. Miner. Deposita 39, 864–889.
Heinrich, C., Driesner, T., Stefansson, A., Seward, T.M., 2004. Magmatic vapor contraction and the transport of gold from porphyry to epithermal ore deposits. Geology 39, 761–764.
Heinrich, C.A., Gunther, D., Audétat, A., Ulrich, T., Frischknecht, R., 1999. Metal fractionation between magmatic brine and vapor, determined by micro-analysis of fluid inclusions. Geology 27, 755–758. https://doi.org/10.1130/0091-7613.
Henley, R.W., McNabb, A., 1978. Magmatic vapor plumes and groundwater interaction in porphyry copper emplacement. Econ. Geol. 73, 1–20. https://doi.org/10.2113/gsecongeo.73.1.1.
Hirayama, K., Haghipour, A., Hajian, J., 1965. Geology of the Zanjan area: The Tarom district, eastern part, with map in scale of 1:100,000. Geol. Surv. Iran, 33 p.
Hirayama, K., Samimi, M., Zahedi, M., Hushmandzadeh, A., 1966. Geology of the Tarom district, western part (Zanjan area, northwest Iran), with 1:100,000 map. Geol. Surv. Iran, Tehran, Report No 8.
John, D.A., 2010. Porphyry Copper Deposit Investigations Report, 5070–B, U.S. Department of the Interior, U.S. Geol. Surv., 186 p.
Kamilli, R.J., Ohmoto, H., 1977. Paragenesis, zoning, fluid inclusion and isotopic studies of the Finlandia Vein, Colqui district, Central Peru. Econ. Geol. 72, 950–982.
Landtwing, M.R., Furrer, C., Redmond, P.B., Pettke, T., Guillong, M., Heinrich, C.A., 2010. The Bingham Canyon porphyry Cu-Mo-Au deposit. III. Zoned copper-gold ore deposition by magmatic vapor expansion. Econ. Geol. 105, 91–118. https://doi.org/10.2113/gsecongeo.105.1.91.
Lecumberri-Sanchez, P., Claiborne Newton, M., Westman, E.C., Kamilli, R.J., Canby, C.M., Bodnar, R.J., et al., 2013. Temporal and spatial distribution of alteration, mineralization and fluid inclusions in the transitional high-sulfidation epithermal–porphyry copper system at Red Mountain, Arizona. J. Geochem. Explor. 125, 80–93. https://doi.org/10.1016/j.gexplo.2012.11.017.
Lowell, J.D., Guilbert, J.M., 1970. Lateral and vertical alteration-mineralization zoning in porphyry ore deposits. Econ. Geol. 65, 373–408. https://doi.org/10.2113/gsecongeo.65.4.373.
Lowenstern, J.B., 2001. Carbon dioxide in magmas and implications for hydrothermal systems. Miner. Deposita 36 (6), 490–502. https://doi.org/10.1007/s001260100185.
Lu, H.Z., Fan, H.R., Ni, P., Ou, X.G., Shen, K., Zhang, W.H., 2004. Fluid inclusion. Science Press, Beijing (in Chinese).
McCammon, C.A., Pnnc, A., Keplsn, H., Snanr, T., 1995. A study of bernalite, $Fe(OH)_3$, using Maassbauer spectroscopy, optical spectroscopy and transmission electron microscopy. Phys. Chem. Minerals 22, 11–20.
Meyer, C., Hemley, J.J., 1967. Wall rock alteration. In: Barnes, H.L. (Ed.), Geochemistry of Hydrothermal Ore Deposits, pp. 166–235.
Moncada, D., Mutchler, S., Nieto, A., Reynolds, T.J., Rimstidt, J.D., Bodnar, R.J., 2012. Mineral textures and fluid inclusion petrography of the epithermal Ag–Au deposits at Guanajuato, Mexico: application to exploration. J. Geochem. Explor. 114, 20–35. https://doi.org/10.1016/j.gexplo.2011.12.001.
Muntean, J.L., Einaudi, M.T., 2000. Porphyry gold deposits of the Refugio district, Maricunga belt, northern Chile. Econ. Geol. 95, 1445–1472.
Muntean, J.L., Einaudi, M.T., 2001. Porphyry-epithermal transition: Maricunga belt, northern Chile. Econ. Geol. 96, 743–772. https://doi.org/10.2113/gsecongeo.96.4.743.
Nabatian, G., Ghaderi, M., 2013. Oxygen isotope and fluid inclusion study of the Sorkhe-Dizaj iron oxide apatite deposit, NW Iran. Int. Geol. Rev. 55, 397–410. https://doi.org/10.1080/00206814.2012.713547.
Nabatian, G., Ghaderi, M., Neubauer, F., Honarmand, M., Liu, X., Dong, Y., Jiang, S.Y., Quadt, A.V., Bernroider, M., 2014. Petrogenesis of Tarom high-potassic granitoids in the Alborz-Azarbaijan belt, Iran: Geochemical, U-Pb zircon and Sr-Nd-Pb isotopic constraints. Lithos 184–187, 324–345.
Nabavi, M.H., 1976. An Introduction to Geology of Iran. Geol. Surv. Iran. 110 (in Persian).
Nash, J.T., 1976. Fluid inclusion petrology, data from porphyry copper deposits and applications to exploration. US Geol. Surv. Prof. Pap. 907D, 16.
Pirajno, F., 2009. Hydrothermal Processes and Mineral Systems. Springer, Berlin, pp. 1250.
Pudack, C., Halter, W.E., Heinrich, C.A., Pettke, T., 2009. Evolution of magmatic vapor to gold-rich epithermal liquid: the porphyry to epithermal transition at Nevados de Famatina, Northwest Argentina. Econ. Geol. 104, 449–477. https://doi.org/10.2113/gsecongeo.104.4.449.
Rankin, A.H., Ramsey, M.H., Coles, B., Van Langevelde, F., Thomas, C.R., 1992. The composition of hypersaline, iron-rich granitic fluids based on laser-ICP and synchrotron-XRF microprobe analysis of individual fluid inclusions in topaz, Mole granite, eastern Australia. Geochim. Cosmochim. Acta 56, 67–79. https://doi.org/10.1016/0016-7037(92)90117-2.
Redmond, P.B., Einaudi, M.T., Inan, E.E., Landtwing, M.R., Heinrich, C.A., 2004. Copper deposition by fluid cooling in intrusion-centered systems: new insights from the Bingham porphyry ore deposit, Utah. Geology 32, 217–220. https://doi.org/10.1130/G19986.1.
Roedder, E., 1971. Fluid inclusion studies on the porphyry-type ore deposits at Bingham, Utah, Butte, Montana, and Climax. Colorado. Econ. Geol. 66, 98–120.
Roedder, E., 1984. Fluid inclusions. In: Reviews in Mineralogy v. 12. Mineral. Soc. Am., Washington, pp. 644.
Roedder, E., Bodnar, R.J., 1997. Fluid inclusion studies of hydrothermal ore deposits. In: Barnes, H.L. (Ed.), Geochemistry of Hydrothermal Ore Deposits, pp. 657–698.
Sahandi, R., 2013. Structural Geology Map of Iran, 1: 1,000,000 Scale. Geol. Surv. Iran.
Seedorff, E., Barton, M.D., Stavast, W.J.A., Maher, D.J., 2008. Root zones of porphyry systems: extending the porphyry model to depth. Econ. Geol. 103, 939–956. https://doi.org/10.2113/gsecongeo.103.5.939.
Seedorff, E., Dilles, J.H., Proffett Jr., J.M., 2005. Porphyry deposits: characteristics and origin of hypogene features. Econ. Geol. 100, 251–298.
Sillitoe, R.H., 2000. Gold-rich porphyry deposits: descriptive and genetic models and their role in exploration and discovery. Rev. Econ. Geol. 13, 315–345.
Sillitoe, R.H., 2005. Supergene oxidized and enriched porphyry copper and related deposits. Econ. Geol. 100, 723–768.
Sillitoe, R.H., 2010. Porphyry copper systems. Econ. Geol. 105, 3–41. https://doi.org/10.2113/gsecongeo.105.1.3.
Sillitoe, R.H., Hedenquist, J.W., 2003. Linkages between volcano-tectonic settings, ore-fluid compositions, and epithermal precious metal deposits. Soc. Econ. Geol. Spec. Publ. 10, 315–343.
Simmons, S.F., White, N.C., John, D.A., 2005. Geological characteristics of epithermal precious and base metal deposits. Econ. Geol. 100, 485–522.
Skinner, B.J., 1997. Hydrothermal mineral deposits: what we do and don't know. In: Barnes, H.L. (Ed.), Geochemistry of Hydrothermal Ore Deposits, third ed. Wiley, New York, pp. 1–29.
Titley, S.R., 1982. The style and progress of mineralization and alteration in porphyry copper systems: American Southwest. In: Titley, S.R. (Ed.), Advances in Geology of the Porphyry Copper Deposits. University of Arizona Press, southwestern North America, Tucson, pp. 93–116.
Tosdal, R.M., Dilles, J.H., Cooke, D.R., 2009. From source to sinks in auriferous magmatic–hydrothermal porphyry and epithermal deposits. Elements 5, 289–295.
Ulrich, T., Gunther, D., Heinrich, C.A., 1999. Gold concentrations of magmatic brines and the metal budget of porphyry copper deposits. Nature 399, 676–679. https://doi.org/10.1038/21406.
Ulrich, T., Gunther, D., Heinrich, C.A., 2001. The evolution of a porphyry Cu-Au deposit based on LA-ICP-MS analyses of fluid inclusions: Bajo de la Alumbrera, Argentina. Econ. Geol. 96, 1743–1774.
Verdel, C., Wernicke, B.P., Hassanzadeh, J., Guest, B., 2011. A Paleogene extensional arc flare-up in Iran. Tectonics 30. https://doi.org/10.1029/2010TC002809.
Vikre, P.G., 1985. Precious metal vein systems in the National District, Humboldt County, Nevada. Econ. Geol. 80 (2), 360–393. https://doi.org/10.2113/gsecongeo.81.4.1023.
Wilkinson, J.J., 2001. Fluid inclusions in hydrothermal ore deposits. Lithos 55, 229–272. https://doi.org/10.1016/S0024-4937(00)00047-5.
Wilkinson, J.J., Rankin, A.H., Mulshaw, S.C., Nolan, J., Ramsey, M.H., 1994. Laser ablation-ICP-AES for the determination of metals in fluid inclusions: an application to the study of magmatic ore fluids. Geochim. Cosmochim. Acta 58, 1133–1146. https://doi.org/10.1016/0016-7037(94)90577-0.
Williams-Jones, A.E., Heinrich, C.A., 2005. Vapor transport of metals and the formation of magmatic-hydrothermal ore deposits. Econ. Geol. 100, 1287–1312.
Yasami, N., Ghaderi, M., Madanipour, S., Taghilou, B., 2017. Structural control on overprinting high-sulfidation epithermal on porphyry mineralization in the Chodarchay deposit, northwestern Iran. Ore Geol. Rev. 86, 212–224. https://doi.org/10.1016/j.oregeorev.2017.01.028.
Yasami, N., Ghaderi, M., Mokhtari, M.A.A., Mousavi Motlagh, S.H., 2018. Petrogenesis of the two phases of intrusive rocks at Chodarchay, NW Iran: using trace and rare earth elements, NW Iran. Arab. J. Geosci 11 (20), 605. https://doi.org/10.1007/s12517-018-3942-3.